LBL-12084

Lawrence Berkeley Laboratory
UNIVERSITY OF CALIFORNIA

Materials & Molecular
Research Division

NONLINEAR OPTICS AT INTERFACES

Chenson K. Chen
(Ph.D. thesis)

December 1980

Prepared for the U.S. Department of Energy under Contract W-7405-ENG-48

LBL-12084

NONLINEAR OPTICS AT INTERFACES

Chenson K. Chen

Ph.D. *Thesis*

December 1980

Materials and Molecular Research Division
Division of Materials Sciences
Lawrence Berkeley Laboratory
University of California
Berkeley, CA 94720

Abstract

NONLINEAR OPTICS AT INTERFACES

Chenson K. Chen

Two aspects of surface nonlinear optics are explored in this thesis. The first part is a theoretical and experimental study of nonlinear interaction of surface plasmons and bulk photons at metal-dielectric interfaces. The second part is a demonstration and study of surface enhanced second harmonic generation at rough metal surfaces.

A general formulation for nonlinear interaction of surface plasmons at metal-dielectric interfaces is presented and applied to both second and third order nonlinear processes. Experimental results for coherent second and third harmonic generation by surface plasmons and surface coherent antiStokes Raman spectroscopy (CARS) are shown to be in good agreement with the theory. In the case of second harmonic generation, it is demonstrated that two counterpropagating surface plasmons at a silver-crystal quartz interface result in a coherent second harmonic output propagating along the surface normal, as required by momentum conservation. In third harmonic generation by a surface plasmon wave propagating along a silver-methanol interface, the result yields the value of the third order nonlinear susceptibility of methanol as $\chi^{(3)}_{1111}(3\omega = \omega + \omega + \omega) \approx 3 \times 10^{-14}$ esu. The work on surface CARS is the first demonstration of a surface nonlinear optical effect in which all input and output waves are surface plasmons. At a silver-benzene interface, the output is resonantly enhanced when the Raman mode of benzene is resonantly excited, and when the output is phase-matched. Just like bulk CARS, surface CARS can be used as a spectro-

scopic tool to probe the Raman resonances of the dielectric. Because of its surface specific nature and short interaction length, the surface CARS technique has the advantage of being able to probe materials with strong absorption and fluorescence, as well as thin films, overlayers, or even adsorbed molecules. The ultimate sensitivity of the surface CARS technique is limited by the damage threshold of the silver film. Even so, by scaling the experimentally observed signal obtained with nanosecond lasers, the surface CARS signal with picosecond laser pulses is expected to have sufficient sensitivity to detect monolayers or even submonolayers of benzene molecules adsorbed to the silver surface.

The second part of the thesis is then focused on nonlinear optical processes at rough metal surfaces. The experimental observation of a 10^4 increase of the second harmonic signal at a rough metal-air interface compared to a smooth surface provides the first unambiguous demonstration that the local field on rough surface structures can lead to a large enhancement in the strength of a nonlinear optical process. The second harmonic output from the roughened surface is angularly diffuse and unpolarized. In addition, a strong broad spectral background on both the Stokes and antiStokes sides of the second harmonic signal is observed. This type of surface enhanced effect is expected to be rather general and should be observable in other nonlinear optical processes. Applications of the effect to the detection and spectroscopic study of adsorbed molecules are speculated.

Acknowledgements

Throughout the course of my graduate career, I received invaluable encouragement and support from fellow members of the Shen group, which I gratefully acknowledge. I would particularly like to thank:

Y. Ron Shen, my thesis advisor, for his guidance, patience, and never ending enthusiasm;

A. Rubens B. de Castro, for working with me throughout the failures and (occasional) successes of my experimental research and for providing the lab with a welcome source of wit and humor; and

Rita Jones, for her invaluable assistance in preparing my thesis.

I would also like to acknowledge my support as an NSF Fellow during my first three years as a graduate student in Berkeley. This work was supported by the Division of Materials Sciences, Office of Basic Energy Sciences, U.S. Department of Energy under contract No. W-7405-ENG-48.

Table of Contents

Introduction

The propagation of surface electromagnetic waves at interfaces has found many applications in the physics of solids and interfaces.[1] They have been used to study adsorbed molecules[2] and overlayers on surfaces,[3] to probe phase transitions,[4] etc. In most cases, linear excitation and detection of surface waves have been used. On the other hand, few observations of nonlinear optical processes involving surface waves have been reported. Simon et al. have used linearly excited surface plasmon waves on metal-air[5] and metal-piezoelectric[6] interfaces to generate bulk second harmonic waves. DeMartini et al. have used the mixing of two bulk waves to generate surface electromagnetic waves,[7] and the mixing of a bulk wave and surface wave as a means of detecting surface waves.[8] Here, experimental results on surface coherent anti-Stokes Raman spectroscopy (CARS), a surface nonlinear process in which all input and output waves are surface plasmons, will be presented and shown to be in good agreement with theoretical prediction.[9] In addition, experimental results on other second and third order nonlinear processes will be discussed. In the process of coherent second harmonic generation by counterpropagating surface plasmons, the second harmonic output will be shown to propagate in a direction normal to the input surface waves.[10]

Following the successful demonstration of the surface CARS technique, attention was then focused on surface enhanced Raman spectroscopy, SERS, in which the spontaneous Raman cross section for certain molecules at roughened metal surfaces was enhanced by 10^5 to 10^6.[11,12] Because the Raman scattering cross section is proportional to the third

order nonlinear susceptibility for CARS processes, the molecules giving rise to the SERS signal were also expected to give rise to an easily observable surface CARS signal. Unfortunately, principally because the high intensity nanosecond laser pulses necessary for surface CARS generation caused desorption of the molecules giving rise to the SERS signal, experimental observation of a surface enhanced surface CARS signal was not successful. However, in an attempt to understand the mechanism giving rise to such a large effect and to isolate the possible effects of metal-molecule interaction, attention was then turned to the possible surface enhancement resulting from local field effects on rough metal surfaces in the absence of any adsorbed molecules. In particular, nonlinear optical processes in metals were considered. Here, experimental results on surface enhanced second harmonic generation at roughened metal surfaces will be presented and interpreted in terms of an electromagnetic local field theory.[13]

In Chapter II, the properties and characteristics of surface plasmons will be reviewed, with an emphasis on physical and intuitive interpretation. In addition, methods for linear excitation and detection of surface plasmons will be discussed. In Chapter III, a general theory for nonlinear interaction of surface plasmons will be formulated and applied to both second and third order nonlinear processes. Detailed comparisons between theory and experiment will be made for both surface CARS and coherent second harmonic generation by counterpropagating surface plasmon experiments. In addition, the ultimate sensitivity and strengths, as well as limitations of the nonlinear surface plasmon technique will be discussed. Finally, in Chapter IV, a brief summary of the numerous SERS theories will be presented. Experimental

results for surface enhanced second harmonic generation will be presented and proposals for supplementary experiments, as well as applications of the surface enhancement effect, will be made.

Chapter II. Linear Properties of Surface Electromagnetic Waves

In this chapter, the character and linear properties of surface electromagnetic waves will be discussed.[1] A simple physical and intuitive description, as well as a detailed mathematical description of surface plasmons will be presented, laying the foundation for subsequent chapters. Typical numbers characterizing surface plasmons at silver-dielectric interfaces as well as a detailed description of the experimental set up used to measure the surface plasmon properties will be given.

A. Single Interface Surface Plasmon

A surface electromagnetic wave is a TM wave which propagates along an interface, with field amplitude a maximum at the interface, and exponentially decaying along the surface normal. Consider an interface at z = 0 (see Fig. 1), separating two semi-infinite isotropic media 1 and 2, with a TM wave propagating along $\hat{x}$. The form of the electric fields are

$$\vec{E}_1 = \vec{\mathcal{E}}_1 e^{ik_x x - \alpha_1 z} e^{-i\omega t} + \text{c.c.} \qquad z \geq 0$$

$$\vec{E}_2 = \vec{\mathcal{E}}_2 e^{ik_x x + \alpha_2 z} e^{-i\omega t} + \text{c.c.} \qquad z \leq 0 \tag{1}$$

$$\vec{\mathcal{E}}_1 = \mathcal{E}_{1x}\left(1,\ 0,\ -\frac{k_x}{k_{1z}}\right) = \mathcal{E}_{1x}\left(1,\ 0,\ i\,\frac{k_x}{\alpha_1}\right)$$

$$\vec{\mathcal{E}}_2 = \mathcal{E}_{2x}\left(1,\ 0,\ -\frac{k_x}{k_{2z}}\right) = \mathcal{E}_{2x}\left(1,\ 0,\ -\,i\,\frac{k_x}{\alpha_2}\right) \tag{2}$$

where k_x is the x component of the wavevector, $k_{1z} = + i\alpha_1$ and $k_{2z} = - i\alpha_2$ are the z components of the wavevector, and ω is the frequency of excitation. By applying the usual boundary conditions, i.e., $E_{\parallel}$ and $D_{\perp}$ must be continuous, for a nontrivial solution, the dispersion relation is, now denoting k_x as K_x

$$\varepsilon_1\alpha_2 + \varepsilon_2\alpha_1 = 0 \tag{3a}$$

or

$$K_x^2 = \frac{\omega^2}{c^2}\frac{\varepsilon_1\varepsilon_2}{\varepsilon_1 + \varepsilon_2} \tag{3b}$$

where K_x is the surface plasmon wavevector, the ε's are the dielectric constants of the media, and $\varepsilon_i \frac{\omega^2}{c^2} = K_x^2 - \alpha_i^2$, $i = 1,2$. Note that for TE waves, a mathematical solution exists only for the unphysical case of exponentially growing field amplitudes. If the fields exponentially decay away from $z = 0$, then either $\varepsilon < 0$ or $K_x > \sqrt{\varepsilon}\,\frac{\omega}{c}$; in either case, then $k_z = \sqrt{\varepsilon \frac{\omega^2}{c^2} - K_x^2}$ will be pure imaginary, corresponding to exponentially decaying fields for the TM case.

Surface plasmons are surface electromagnetic waves occuring at a metal-dielectric interface, with dielectric constants ε_m and ε_d respectively. If $\varepsilon_m = 1 - \frac{\omega_p^2}{\omega^2}$ where ω_p is equal to the plasma frequency of the metal, then from Eq. (3), the dispersion curve for surface plasmons can be calculated as shown in Fig. 2; in fact, surface plasmons exist only if $|\varepsilon_m| > \varepsilon_d > 0$, $\varepsilon_m < 0$, or equivalently in the region $0 < \omega < \frac{\omega_p}{\sqrt{1 + \varepsilon_d}}$. In reality, ε_m cannot always be modeled by a lossless free electron plasma model, but the condition $|\varepsilon_m| > \varepsilon_d > 0$, $\varepsilon_m < 0$ is a

sufficient condition for the existence of a surface plasmon. Furthermore, the damping of the metal introduces damping into the surface plasmon; if $\varepsilon_m = \varepsilon_m' + i\varepsilon_m''$, then $K_x = K_x' + iK_x''$, where

$$K_x' \cong \frac{\omega}{c}\sqrt{\frac{\varepsilon_m'\varepsilon_d}{\varepsilon_m' + \varepsilon_d}}$$

$$K_x'' \cong \frac{\left(\frac{\omega}{c}\right)^2}{2K_x'} \frac{\varepsilon_m''\varepsilon_d^2}{(\varepsilon_m' + \varepsilon_d)^2} \tag{4}$$

in the limit $\varepsilon_m'' \ll |\varepsilon_m'|$. Thus, as the surface plasmon propagates along $\hat{x}$, its field amplitude decays as $|e^{i(K_x'+iK_x'')x}| = e^{-K_x''x}$.

Finally, it is instructive to calculate the Poynting vector for surface plasmons, both in the metal and in the dielectric medium. Using the Maxwell equations ($\mu = 1$)

$$\vec{\mathcal{H}}_m = |\vec{\mathcal{E}}_m|(0, \sqrt{\varepsilon_m}, 0)$$

$$\vec{\mathcal{H}}_d = |\vec{\mathcal{E}}_d|(0, \sqrt{\varepsilon_d}, 0) \tag{5}$$

and using $\vec{S} = \frac{c}{2\pi}\,\mathrm{Re}(\vec{\mathcal{E}} \times \vec{\mathcal{H}}^*)$,

$$\vec{S}_m = -\hat{x}\,\frac{c}{2\pi}\,|\vec{\mathcal{E}}_m|^2\,\frac{K_x}{\frac{\omega}{c}}\,e^{-2K_x''x}e^{-2\alpha_m z} \qquad z \geqslant 0$$

$$\vec{S}_d = +\hat{x}\,\frac{c}{2\pi}\,|\vec{\mathcal{E}}_d|^2\,\frac{K_x}{\frac{\omega}{c}}\,e^{-2K_x''x}e^{+2\alpha_d z} \qquad z \leqslant 0. \tag{6}$$

Because $\alpha_m > \alpha_d > 0$, and for surface plasmons,

$$\frac{|\vec{\mathcal{E}}_d|^2}{|\vec{\mathcal{E}}_m|^2} = \frac{|\varepsilon_m|}{|\varepsilon_d|} \tag{7}$$

and $|\varepsilon_m| > \varepsilon_d > 0$, although energy in the metal propagates antiparallel to the surface plasmon, i.e., along $-\hat{x}$, the total or net energy flow is dominated by $\vec{S}_d$ in the $+\hat{x}$ direction, parallel to the surface plasmon propagation direction.

From the above discussion, it is evident that surface plasmons can provide a very useful surface probe. First, because energy is confined to a thickness along the surface normal $\sim \frac{1}{\alpha} < \lambda$, the field intensities at the interface can be very large. Not only are the high field intensities of prime importance for nonlinear processes, but also, they make surface plasmons very sensitive to adsorbed molecules[2] and molecular monolayers.[3] Also, from the dispersion relation, one can see that surface plasmons are very sensitive to changes in the dielectric properties of the media;[4,14] furthermore, because of the relatively large damping of the metal, surface plasmons are very insensitive to the absorption or scattering losses in the dielectric media, and for example, can be used to study absorbing media and phase transitions.[4]

B. The Attenuated Total Reflection Technique

Although Sommerfeld recognized the existence of surface plasmons in 1909,[15] it was not until 1968, when Otto developed the ATR (attenuated total reflection) technique[16] that the study of surface plasmons became popular. As a modified version of the Otto method, the Kretschmann ATR configuration,[17] developed in 1971, has provided an extremely convenient and useful experimental tool with which one can probe metal-dielectric interfaces. Here, a brief review of the ATR technique will be presented, with physical explanations of the formalism, as well as a simple conservation of energy consideration in estimating the actual

enhancements of the electric field.

The basic principle of ATR is very simple. In order to excite a surface plasmon at a metal-dielectric interface, k_x must be $> \sqrt{\varepsilon_d}\,\frac{\omega}{c}$. If one incorporates a third medium, as shown in Fig. 3, a prism with $\varepsilon_p > \varepsilon_d$, then at an appropriate angle of incidence, i.e., $\frac{\omega}{c}\sqrt{\varepsilon_p}\sin\theta_{sp} = K'_x$, it is possible to excite a surface plasmon at the metal-dielectric interface. Furthermore, if the thickness of the metal film, d, is appropriately chosen, then for a TM wave incident on the prism-metal interface, one can achieve 100% coupling to the surface plasmon at the metal-dielectric interface. By monitoring the magnitude of the reflected beam as a function of angle θ, a minimum in the reflectivity will occur at θ_{sp} (see, for example, Fig. 4), and the width of the reflectivity dip will be proportional to the damping, K''_x of the surface plasmon.

The dispersion relation for a surface plasmon in the Kretschmann ATR configuration can be easily calculated by considering the appropriate forms for the TM electric fields and applying the appropriate boundary conditions. Consider the two interface geometry, with prism $z \geq d$, metal, $0 \leq z \leq d$, and dielectric $z \leq 0$, Fig. 3, with a surface plasmon propagating along $\hat{x}$. Then, the fields are of the form

$$\vec{E}_p = \vec{\mathcal{E}}_p e^{ik_x x - \alpha_p (z-d)} e^{-i\omega t}$$

$$\vec{E}_m = \vec{\mathcal{E}}_{m1} e^{ik_x x + \alpha_m z} e^{-i\omega t} + \vec{\mathcal{E}}_{m2} e^{ik_x x - \alpha_m z} e^{-i\omega t}$$

$$\vec{E}_d = \vec{\mathcal{E}}_d e^{ik_x x + \alpha_d z} e^{-i\omega t} \qquad (8)$$

where the subscripts p, m, d refer to prism, metal, and dielectric respectively. By requiring that $(\vec{E})_{\parallel}$ and $(\vec{D})_{\perp}$ be continuous at z = 0 and z = d, and using $\nabla \cdot \vec{E} = 0$ for isotropic media to relate the components of the fields, a nontrivial solution exists for $\vec{\mathcal{E}}_p$, $\vec{\mathcal{E}}_{m1}$, $\vec{\mathcal{E}}_{m2}$, $\vec{\mathcal{E}}_d$ only if

$$D(\omega, k_x = K_x) = 0$$

$$D(\omega,k_x) = (\varepsilon_m\alpha_d+\varepsilon_d\alpha_m)(\varepsilon_p\alpha_m+\varepsilon_m\alpha_p) + e^{-2\alpha_m d}(\varepsilon_m\alpha_d-\varepsilon_d\alpha_m)(\varepsilon_p\alpha_m-\varepsilon_m\alpha_p). \quad (9)$$

Note that if $e^{-2\alpha_m d} \ll 1$, which it is in the usual Kretschmann case, then, by comparing Eq. (9) and Eq. (3), it is evident that the presence of the prism merely acts as a minor perturbation to the zeroth order surface plasmon dispersion relation at the metal-dielectric interface. The ATR configuration is useful in exciting surface plasmons only if $K_x' < k_p = \sqrt{\varepsilon_p}\,\frac{\omega}{c}$. In this case, $k_{pz} = \sqrt{k_p^2 - K_x'^2}$ is pure real, and causes the surface plasmon at the metal-dielectric interface to have a radiative loss; in otherwords, as the surface plasmon propagates along the interface, its amplitude decays via two processes: 1) internal damping in the metal, and 2) radiative damping by coupling to bulk em waves in the prism. In fact, the dispersion relation $D(\omega,k_x) = 0$ can be written as

$$K_x \cong K_{xo} + k_{rr} + i(k_{ii} + k_{ir}) \quad (10)$$

where

$$K_{xo} \cong \frac{\omega}{c}\sqrt{\frac{\varepsilon'_m \varepsilon_d}{\varepsilon'_m + \varepsilon_d}} \tag{11a}$$

$$k_{ii} \cong \left(\frac{\omega}{c}\right)^2 \frac{\varepsilon''_m \varepsilon_d^2}{2K_{xo}(\varepsilon'_m + \varepsilon_d)^2} \tag{11b}$$

$$k_{rr} \cong \frac{\omega}{c} \frac{2\varepsilon'_m \alpha_d}{K_{xo}\left(\varepsilon'^2_m - \varepsilon_d^2\right)} e^{-2\alpha_m d} \mathrm{Re}(r_{pm}) \tag{11c}$$

$$k_{ir} \cong \frac{\omega}{c} \frac{2\varepsilon'_m \alpha_d}{K_{xo}\left(\varepsilon'^2_m - \varepsilon_d^2\right)} e^{-2\alpha_m d} \mathrm{Im}(r_{pm}) \tag{11d}$$

where r_{pm} is the Fresnel coefficient for reflection of a TM wave from a prism-metal interface, and $\left|\frac{\varepsilon''_m}{\varepsilon'_m}\right|$, $e^{-2\alpha_m d} \ll 1$.

Having calculated the surface plasmon dispersion relation for a prism-metal-dielectric interface, the next logical step is to consider how the surface plasmon can be excited. Physically, from momentum considerations, for a TM wave incident on the prism side, if $k_x = K_{xo} + k_{rr}$, where k_x is the x component of the incident wave vector, then one would expect that the surface plasmon at the metal-dielectric interface would be resonantly excited. Formally, the linear excitation of a surface plasmon by the ATR technique can be completely described by linear Fresnel coefficients. For a TM wave,

$$\vec{E}_{inc} = \vec{\mathcal{E}}_{inc} e^{ik_x x + ik_{pz}(z-d)} e^{-i\omega t} + \text{c.c.} \tag{12}$$

incident on the prism side of the Kretschmann ATR prism-metal-dielectric geometry, the linear Fresnel reflection and transmission coefficients are given by

$$r_{pmd} = \frac{|\vec{\mathcal{E}}_p|}{|\vec{\mathcal{E}}_{inc}|} = \frac{r_{pm} + e^{2ik_{mz}d} r_{md}}{1 + e^{2ik_{mz}d} r_{pm} r_{md}} \tag{13}$$

and

$$t_{pmd} = \frac{|\vec{\mathcal{E}}_d|}{|\vec{\mathcal{E}}_{inc}|} = \frac{t_{pm} t_{md} e^{ik_{mz}d}}{1 + e^{2ik_{mz}d} r_{pm} r_{md}} \tag{14}$$

where

$$r_{pm} = \frac{\varepsilon_m k_{pz} - \varepsilon_p k_{mz}}{\varepsilon_m k_{pz} + \varepsilon_p k_{mz}} \tag{15}$$

and

$$t_{pm} = \frac{2\sqrt{\varepsilon_p \varepsilon_m}\, k_{pz}}{\varepsilon_m k_{pz} + \varepsilon_p k_{mz}} \tag{16}$$

and p,m replaced by m,d respectively for r_{md} and t_{md}.[18] In their present form, the Fresnel coefficients provide little or no insight about surface plasmons. However, with appropriate substitutions and algebraic manipulation, the Fresnel coefficients can be rewritten in a much more intuitive form. The first important observation to be made is that if

$$k_{pz} = -i\alpha_p$$

$$k_{mz} = -i\alpha_m$$

$$k_{dz} = -i\alpha_d, \tag{17}$$

then the denominators of r_{pmd} and t_{pmd} are exactly equivalent to $D(\omega, k_x)$; thus, when surface plasmons are excited, r_{pmd} and t_{pmd} have resonant denominators. Second, consider the wavevectors present when the ATR geometry is used, i.e., $k_{mz} = -i\alpha_m$, $k_{dz} = -i\alpha_d$, and k_{pz}, α_m, and α_d are real. For $k_x \cong K'_x$, then $|r_{pmd}|^2$ can be written as

$$R \equiv |r_{pmd}|^2 \cong 1 - \frac{4k_{ii}k_{ir}}{|\delta k - i(k_{ii} + k_{ir})|^2} \tag{18}$$

where $\delta k = k_x - K'_x \cong k_x - (K_{xo} + k_{rr})$ and $k_x = \frac{\omega}{c}\sqrt{\varepsilon_p}\sin\theta$. Thus, if the thickness of the metal film is chosen such that the radiative and intrinsic damping are equal, i.e., $k_{ii} = k_{ir}$, then, when $\delta k = 0$, $R = 0$, and all of the incident light energy is coupled to the surface plasmon. Furthermore, by measuring $R(\theta)$, the width of the reflectivity dip gives a direct measure of the damping of the surface plasmon, $k_{ii} + k_{ir}$. At first sight, it seems somewhat contradictory that $k_{ii} = k_{ir}$, and yet, there is no reflected wave. Physically, the explanation is simply that the surface plasmon does have a radiative loss, but it interferes destructively with the electric field that is reflected from the initial p-m interface (in practice, the term $e^{-2\alpha_m d}$ makes multiple reflections much less important). Thus, ultimately, all of the energy of the surface plasmon is lost by damping in the metal film.

Similarly, consider the enhancement factor t_{pmd} or $T \equiv |t_{pmd}|^2$. With the same substitutions and approximations,

$$t_{pmd} \cong \frac{4\varepsilon_p^{\frac{1}{2}}\varepsilon_d^{\frac{3}{2}}\varepsilon_m k_{pz}\alpha_m^2 e^{-\alpha_m d}}{(\varepsilon_m k_{pz} + i\varepsilon_p\alpha_m)(\varepsilon_d^2 - \varepsilon_m^2)K'_x[\delta k - i(k_{ii} + k_{ir})]} . \tag{19}$$

In the case that $k_{ii} = k_{ir}$ and when $\delta k = 0$, by using Eq. (11b) and

(11d) to express $e^{-\alpha_m d}$ in terms of the k's, α's, and ε's, T can be expressed in a much more simple form,

$$T_{max} \cong \left| \frac{K_x k_{pz}}{\frac{\omega^2}{c^2}(\varepsilon_d - \varepsilon_m)} \times \frac{\alpha_m}{k_{ii}} \right| . \qquad (20)$$

Thus, as one would expect, the maximum enhancement occurs when the surface plasmon is resonantly excited, and is inversely proportional to the damping of the surface plasmon.

Alternatively, one should be able to calculate the enhancement factor from simple physical considerations, namely energy conservation. Consider infinite plane waves incident on the Kretschmann ATR geometry, Fig. 3, with the thickness d of the metal film chosen so that $R(\theta = \theta_{sp}) = 0$. In the metal and dielectric, the Poynting vector, $\vec{S}$, has components only along $\pm \hat{x}$. Furthermore, because $|\vec{\mathcal{E}}_p|$ = reflected field = 0 at $\theta = \theta_{sp}$, there is no energy radiated from the metal film by the surface plasmon field. The power loss/volume of the surface plasmon as it propagates along $\hat{x}$ is given by

$$P_{sp,loss}/\text{volume} = (S_x(x) - S_x(x + dx)) \frac{dydz}{dxdydz}$$

$$= 2K''_x S_x \qquad (21)$$

where $K''_x = k_{ii}$. In the above approximation, because no energy is lost via radiative damping, it is appropriate to choose the damping parameter to be k_{ii} as in Eq. (11b) for the single interface surface plasmon. The total energy loss/time in a volume element $dxdy\int dz$ at $x = 0$, using Eq. (6) is given by

$$P_{sp,loss} = dxdy \int_{-\infty}^{\infty} dz \; 2K_x'' S_x$$

$$\cong 2K_x'' dxdy \left[\int_{-\infty}^{0} S_{x,d} dz + \int_{0}^{\infty} S_{x,m} dz \right]$$

$$= \frac{k_{ii} K_x}{\frac{\omega}{c}} \left[\frac{|\vec{\mathcal{E}}_d|^2}{\alpha_d} - \frac{|\vec{\mathcal{E}}_m|^2}{\alpha_m} \right] \frac{c}{2\pi} \, dxdy$$

$$= \frac{k_{ii} K_x}{\frac{\omega}{c}} \left[\frac{1}{\alpha_d} + \frac{\epsilon_d}{\epsilon_m \alpha_m} \right] \frac{c}{2\pi} |\vec{\mathcal{E}}_d|^2 dxdy. \qquad (22)$$

Furthermore, because the energy propagating along + $\hat{x}$ leaving the volume element dxdy $\int dz$ at x + dx is exactly compensated by the energy propagating along + $\hat{x}$ entering the same volume element at x, there is no net energy radiated from the volume element under consideration. On the other hand, the total energy input/time into the same volume element by $\vec{\mathcal{E}}_{inc}$ is given by

$$P_{inc} = \frac{c}{2\pi} \sqrt{\epsilon_p} |\vec{\mathcal{E}}_{inc}|^2 dxdy \cos\theta_{sp}. \qquad (23)$$

Because there can be no energy build up in any volume element in the steady state case, energy conservation requires $P_{inc} = P_{sp,loss}$. Thus, by using Eq. (3) and recognizing that $|k_{pz}| = |\sqrt{\epsilon_p} \frac{\omega}{c} \cos\theta_{sp}|$

$$\frac{|\vec{\mathcal{E}}_d|^2}{|\vec{\mathcal{E}}_{inc}|^2} = \left| \frac{K_x' k_{pz}}{\left(\frac{\omega}{c}\right)^2 (\epsilon_d - \epsilon_m)} \cdot \frac{\alpha_m}{k_{ii}} \right|, \qquad (24)$$

which is identical to the expression derived from the exact Fresnel transmission coefficient, Eq. (20).

Having developed the formalism characterizing the linear proper-

ties of surface plasmons, it is now instructive to consider what materials are most useful in exciting surface plasmons and then to calculate typical realistic values for the field enhancement factor and surface plasmon propagation lengths. For excitation in the visible and near IR, silver and gold are the best metals because of their relatively weak damping and large dielectric constants, $|\varepsilon_m| \gg 1$. Silver has the least damping of any metal in this region and thus yields surface plasmons with relatively large enhancement factors. Gold, on the other hand, is a relatively inert metal, and can be used with relatively less stable dielectric materials, e.g. liquid crystals. Because of the excitation mechanism for the ATR technique, it is apparent that surface plasmons can be excited only for dielectrics with $\varepsilon_d < \varepsilon_p$. Thus, it is imperative to choose a prism with high index of refraction. Although higher refractive index materials are available, such as $LiNbO_3$ or rutile, heavy flint glass prisms, Schott F2 or SF10, were used because they possessed inversion symmetry (important for nonlinear experiments), were chemically stable, were commercially available, and were relatively inexpensive. For typical numbers, consider the Kretschmann ATR geometry, prism-silver film-dielectric for two cases, $\varepsilon_d = 1$ for air and $\varepsilon_d = 2.25$ for a typical organic liquid, e.g. benzene, and $\varepsilon_p = 3.0$. For an incident field at $\lambda = 6328$ Å, $\varepsilon_m \cong -20 + i\,1.0$[19] and in either case, a silver film of ~ 500 Å thickness will provide near optimal coupling to the surface plasmon. Using Eq. (19) or (20), for $\varepsilon_d = 1$, $|t_{pmd}| \sim 15$. In the case $\varepsilon_d = 2.25$, one finds that $|t_{pmd}| \sim 7$ and $k_{ii} \sim \frac{\omega}{c} \times 5 \times 10^{-3}$; this corresponds to $\Delta\theta_{FWHM} \sim 1.2°$ in the reflectivity dip $R(\theta)$, with θ defined at the metal-prism interface, and a propagation length $\frac{1}{K''_x} \sim 10$ μm. Experimentally, it has been determined that

faster evaporation rates for silver, up to at least 50 Å/sec, will produce narrower surface plasmon reflectivity dips.

The experimental set up used to monitor the surface plasmon excitation is shown in Fig. 5. With the incident beam fixed in space, as the prism-mirror assembly is rotated, the reflected beam is translated, but always propagates in the same direction. Note that it is not necessary for the mirror to be parallel to the silvered prism surface. Thus, by placing a detector at the focal point of the collection lens as shown, the reflectivity of the incident beam can be monitored, directly measuring $R(\theta)$. As a note of caution, in comparing the measured reflectivity to $R(\theta)$ given in Eq. (13), one must include the reflectivity losses at the prism-air interface as well as the mirror-air interface. Although the major dependence is given by $R(\theta)$, the additional factors slightly alter the wings and shoulders of the measured reflectivity. A Responsyn HDM155 stepping motor was used to control the rotary table, with a 0.05 degree step size. An E G and G SGD 100 A photodiode with a - 90 volt bias was used to measure the reflected beam; for CW lasers, the photodiode output was directly recorded by a HP680M strip chart recorder; for pulsed lasers, the photodiode output was integrated by a gated electrometer and then recorded on a strip chart recorder. 99.95% pure silver was used to evaporate the thin metal films onto F2 or SF10 glass equilateral prisms (30 mm × 30 mm) available from Klinger Scientific Corporation. The prism was mechanically mounted on the rotary table, and a cell with a teflon O-ring seal was pressed against the silvered prism face, providing a liquid reservoir.

In summary, a brief review of surface plasmons has been presented. Physical interpretations as well as a simple conservation of energy

argument have been used to give the reader a simple intuitive understanding of surface plasmons. Furthermore, it was shown that from a measured ATR reflectivity curve, one can calculate realistic values of surface plasmon characteristics.

Chapter III. Nonlinear Interaction of Surface Plasmons at Metal-Dielectric Interfaces

Although nonlinear optics in bulk media is a well developed field, surface nonlinear optics, in particular, nonlinear interaction of surface plasmons, has been relatively unexplored. Physically, because the surface plasmon fields are strongly enhanced, surface nonlinear optical processes can be easily observed. In this chapter, a general formalism of nonlinear surface plasmon interaction, exact within the framework of the nonlinear Maxwell equations, will be presented, and then applied to both $\chi^{(2)}$ and $\chi^{(3)}$ processes in which theory and experiment can be directly compared. The ultimate sensitivity and potential, as well as possible limitations of the nonlinear surface plasmon technique for material studies will be discussed.

A. General Theory

The theory of nonlinear interaction of surface plasmons is a straight forward extension of the theory on nonlinear generation and detection of surface plasmons developed earlier.[20,21] Consider the Kretschmann ATR geometry as shown in Fig. 3. The dispersion relation of the surface plasmons is given by Eq. (9)

$$D(\omega, k_x = K_x) = 0,$$

where

$$D(k_x,\omega) = (\varepsilon_m\alpha_d + \varepsilon_d\alpha_m)(\varepsilon_p\alpha_m + \varepsilon_m\alpha_p) + e^{-2\alpha_m d}(\varepsilon_m\alpha_d - \varepsilon_d\alpha_m)(\varepsilon_p\alpha_m - \varepsilon_m\alpha_p), \quad (25)$$

where the subscripts p, m, and d refer to the prism, metal, and dielectric, respectively, the ε's are the dielectric constants, $\alpha_p^2 = k_x^2 - \varepsilon_p \times \frac{\omega^2}{c^2}$, $\alpha_m^2 = k_x^2 - \varepsilon_m \frac{\omega^2}{c^2}$, and $\alpha_d^2 = k_x^2 - \varepsilon_d \frac{\omega^2}{c^2}$, d is the thickness of the metal film, and $K_x = K_x' + iK_x''$ is the complex wavevector of the surface plasmon. Let $\vec{E}_{pi}$, $i = 1,2,\ldots,n$ be the incident fields at frequencies ω_i, and $\vec{E}_{di}$ be the field associated with the surface plasmon in the dielectric medium, where $|\vec{E}_{di}| = t_i|\vec{E}_{pi}|$ and $t_i = t_{pmd}$ is the enhancement associated with the surface plasmon fields. Then the nonlinear generation is governed by the nonlinear Maxwell equation

$$\left(\nabla \times \nabla \times - \frac{\omega^2}{c^2}\varepsilon\right)\vec{E} = \begin{cases} 4\pi \frac{\omega^2}{c^2}\vec{P}^{(NL)} & z \leq 0 \\ 0 & z \geq 0 \end{cases}$$

and

$$\nabla \cdot \vec{D} = 0 \tag{26}$$

with the proper boundary conditions applied at $z = 0$ and $z = d$, where $\vec{P}^{(NL)} = \overleftrightarrow{\chi}^{(NL)} : \vec{E}_{d1}\vec{E}_{d2} \cdots \vec{E}_{dn}$ and $\vec{D} = \varepsilon\vec{E} + 4\pi\vec{P}^{(NL)}$. Here only isotropic media will be considered, and the dielectric ($z \leq 0$) will be assumed to be the only nonlinear medium. The case in which the nonlinearity of the metal is important, can be similarly solved. In general, the form of the solution is given by

$$\vec{E}_p = \vec{\mathcal{E}}_p e^{ik_x x + ik_{pz}(z-d)} e^{-i\omega t} + \text{c.c.} \qquad z \geq d$$

$$\vec{E}_m = \vec{\mathcal{E}}_{m1} e^{ik_x x + ik_{mz} z} e^{-i\omega t} + \vec{\mathcal{E}}_{m2} e^{ik_x x - ik_{mz} z} e^{-i\omega t} + \text{c.c.} \qquad 0 \leq z \leq d \tag{27}$$

and

$$\vec{E}_d = \vec{\mathcal{E}}_d e^{ik_x x + ik_{dz} z} e^{-i\omega t} + \vec{\mathscr{P}} e^{ik_x x + ik_{sz} z} e^{-i\omega t} + \text{c.c.} \qquad z \leq 0 \qquad (27)$$

where $\vec{\mathcal{E}}_p$, $\vec{\mathcal{E}}_{m1}$, $\vec{\mathcal{E}}_{m2}$, and $\vec{\mathcal{E}}_d$ are the homogeneous solutions and $\vec{\mathscr{P}}$ is the particular solution to the Maxwell equations, k_x is the x component of the wavevector, $k_{pz}^2 = k_p^2 - k_x^2 = -\alpha_p^2$, $k_{mz}^2 = k_m^2 - k_x^2 = -\alpha_m^2$, $k_{dz}^2 = k_d^2 - k_x^2 = -\alpha_d^2$, $k_p^2 = \varepsilon_p \frac{\omega^2}{c^2}$, $k_m^2 = \varepsilon_m \frac{\omega^2}{c^2}$, $k_d^2 = \varepsilon_d \frac{\omega^2}{c^2}$, $\vec{k}_s = \vec{k}_1 + \vec{k}_2 + \ldots + \vec{k}_n$, and $\omega = \omega_1 + \omega_2 + \ldots + \omega_n$. $\vec{\mathscr{P}}$ can be solved directly from the wave equation for $z \leq 0$, and the homogeneous solutions can then be solved by applying the boundary conditions $E_{\|}$ and $B_{\|}$ continuous at $z = 0$ and $z = d$ and using $\nabla \cdot \vec{E} = 0$ to relate the field components. The solution for the TM case for $\vec{\mathcal{E}}_p$ and $\vec{\mathcal{E}}_d$ at frequency ω is given by

$$|\vec{\mathcal{E}}_d| = \left| \frac{4\pi k_m^2}{k_d\left(k_s^2 - k_d^2\right)} \times \frac{\mathscr{A}}{D(k_x,\omega)} \right|$$

$$\mathscr{A} = \left\{ P_x^{(NL)}\left(k_s^2 - k_d^2\right) + \left(k_{sz} P_x^{(NL)} - k_x P_z^{(NL)}\right)\left(\frac{\varepsilon_d k_{mz}}{\varepsilon_m} - k_{sz}\right) \right\}$$

$$\times \left(\varepsilon_m k_{pz} + \varepsilon_p k_{mz}\right) + e^{2ik_{mz}d} \left\{ P_x^{(NL)}\left(k_s^2 - k_d^2\right) + \left(k_{sz} P_x^{(NL)}\right.\right.$$

$$\left.\left. - k_x P_z^{(NL)}\right)\left(\frac{\varepsilon_d k_{mz}}{\varepsilon_m} + k_{sz}\right) \right\} \times \left(\varepsilon_m k_{pz} - \varepsilon_p k_{mz}\right) \qquad (28)$$

$$|\vec{\mathcal{E}}_p| = \left| 8\pi k_{mz} k_p \varepsilon_m \frac{\mathscr{B} e^{ik_{mz}d}}{D(k_x,\omega)} \right|$$

$$\mathscr{B} = \frac{k_{dz} P_x^{(NL)} + k_x P_z^{(NL)}}{k_{sz} + k_{dz}} . \qquad (29)$$

At this point, a few comments about the physical aspects contained

within the mathematical formalism would be helpful. The mechanism leading to the nonlinear generation is very straightforward. The incident fields $\vec{\mathcal{E}}_{pi}$ excite surface plasmons at ω_i at the metal-dielectric interface. The surface plasmon fields then generate a nonlinear polarization, $\vec{P}^{(NL)}$ at $\omega = \omega_1 + \omega_2 + \ldots + \omega_n$, in the dielectric medium, and $\vec{P}^{(NL)}$, in turn, radiates, generating the output fields $\vec{\mathcal{E}}_d$ and $\vec{\mathcal{E}}_p$. The nonlinear enhancement of the output fields resulting from the surface plasmon enhancement of the incident fields is shown explicitly in the expression for $\vec{P}^{(NL)}$ as the product of the input surface plasmon fields $\vec{E}_{d1}\vec{E}_{d2}\ldots\vec{E}_{dn}$. Furthermore, as in bulk nonlinear optics, any material resonance will be contained in the expression for $\overleftrightarrow{\chi}^{(NL)}$; for example, $\overleftrightarrow{\chi}^{(3)}$ may contain a resonant denominator in the case of a Raman active medium. Finally, it is important to note that if it is possible to phase match the nonlinear field, i.e. the output wave is also a surface plasmon, then the term $(D(k_x,\omega))^{-1}$ will provide an additional resonant denominator.

B. Coherent Second Harmonic Generation by Counterpropagating Surface Plasmons

The simplest surface nonlinear optical process, second harmonic generation, involving a single surface plasmon input, was first observed by Simon et al. in 1974.[5] In that case, surface plasmons were excited at a silver-air interface, and the nonlinearity was interpreted as arising from a surface dipole layer in the silver film. By exciting surface plasmons at a silver-piezoelectric crystal (quartz or KDP) interface, because $\chi^{(2)} \neq 0$ in the electric dipole (El) approximation, Simon et al. observed a much larger second harmonic signal.[6] Here, ex-

perimental results on coherent second harmonic generation by counterpropagating surface plasmons will be presented.[10] In a bulk nonlinear medium, counterpropagating waves will lead to second harmonic generation in all directions. On the surface, however, because of the requirement of conservation of wavevector along the surface, counterpropagating surface waves generate coherent second harmonic waves only in the direction perpendicular to the surface. This peculiar effect has been pointed out earlier by several authors in a number of theoretical studies.[22] On the other hand, experimentally, second harmonic generation propagating in a direction perpendicular to the surface has been generated by counterpropagating evanescent[23] and guided waves,[24] but not by surface plasmons.

The surface plasmons along a silver-crystal quartz interface were excited by using a slightly modified Kretschmann geometry, as shown in Fig. 6(a). In this case, the nonlinearity of the quartz was mainly responsible for the second harmonic generation. The quartz crystal was oriented with its $\hat{a}$ axis along $\hat{x}$ and its $\hat{b}$ axis along $\hat{z}$. The two surface plasmon waves

$$\left.\begin{aligned} \vec{E}_1 &= \vec{\mathcal{E}}_1 e^{ik_{1x}+\alpha_1 z} e^{-i\omega t} + \text{c.c.} \\ \vec{E}_2 &= \vec{\mathcal{E}}_2 e^{-ik_{1x}+\alpha_1 z} e^{-i\omega t} + \text{c.c.} \end{aligned}\right\} z \leq 0 \qquad (30)$$

generated a nonlinear polarization

$$\vec{P}^{(2)} = \hat{x}\, d_{11}(\mathcal{E}_{1x}\mathcal{E}_{2x} - \mathcal{E}_{1z}\mathcal{E}_{2z}) e^{2\alpha_1 z} e^{-i2\omega t} \qquad (31)$$

where $d_{11} = \chi^{(2)}_{xxx}$ is the nonlinear susceptibility of quartz, and the field amplitudes $|\vec{\mathcal{E}}_{1,2}|$ are related to the incident field amplitudes in the prism by the usual Fresnel transmission coefficient, using Eq. (14). Using the formalism developed in Eqs. (26) and (29),

$$\vec{E}_q = \vec{\mathcal{E}}_q e^{-ik_q z} e^{-i2\omega t} + \text{c.c.} \tag{32}$$

where $k_x = 0$ and $k_{qz} = -k_q = -\sqrt{\varepsilon_q}\,\frac{2\omega}{c}$, and the power radiated in the quartz is given by

$$\mathcal{P}(2\omega) = \frac{c}{2\pi}\sqrt{\varepsilon_q}\, A\, |F|^2 \left| \frac{4\pi\left(\frac{2\omega}{c}\right)^2 p^{(2)}_x}{4\alpha_1^2 + \left(\frac{2\omega}{c}\right)^2 \varepsilon_q} \right|^2$$

$$F = \frac{\varepsilon_m k_q}{\alpha_m} \left[\frac{(\varepsilon_m k_p + i\varepsilon_p \alpha_m)(\alpha_m + 2\alpha_1) + (\varepsilon_m k_p - i\varepsilon_p \alpha_m)(2\alpha_1 - \alpha_m) e^{-2\alpha_m d}}{(\varepsilon_m k_p + i\varepsilon_p \alpha_m)(-\varepsilon_m k_q + i\varepsilon_q \alpha_m) + (\varepsilon_m k_p - i\varepsilon_p \alpha_m)(\varepsilon_m k_q + i\varepsilon_q \alpha_m) e^{-2\alpha_m d}} \right] \tag{33}$$

where the subscript q for quartz has replaced subscript d, and A is the beam overlap area at the interface. Physically, the two incident laser beams excited two counterpropagating surface plasmons at the silver-crystal quartz interface. The two surface plasmons then interacted via $\vec{\vec{\chi}}^{(2)}$ of the quartz, generating a nonlinear polarization, $\vec{P}^{(NL)}(2\omega)$, which in turn radiated, generating second harmonic photons. Furthermore, because of the requirement of conservation of momentum along the interface, $k_x(2\omega) = k_{1x} + k_{2x} = 0$; hence, bulk photons were coherently generated only in directions normal to the interface, i.e. along $\hat{z}$.

The experimental arrangement is shown in Fig. 6(b). A dye laser oscillator-amplifier system, with NK-199 in acetone, pumped by a Q-switched ruby laser, provided 7-mJ, 20-nsec laser pulses at 10 pulses/

minute. The laser beam was tuned to 7456 Å with a linewidth less than 1 cm^{-1}, and was linearly polarized in the $\hat{x} - \hat{z}$ plane. The sample assembly was mounted on a rotary table, and consisted of an equilateral Schott SF-10 glass prism, a layer of α-bromonapthalene as index matching fluid, and a ~ 500 Å silver film evaporated on a crystalline quartz substrate. The dye laser beam was directed to the sample assembly as shown in Fig. 6(b). In order to provide a counterpropagating surface plasmon wave, the laser beam exiting from the prism was reflected back onto itself. Intensities of the two beams and the efficiency of surface plasmon excitation were monitored through beam splitters in the laser beams. The second harmonic signal was detected on the quartz side along the surface normal direction.

The experimental results are shown in Fig. 7 in comparison with theory, with the second harmonic signal plotted as a function of angle. Each data point represents an average of 10 shots. The observed maximum occurs, as expected, at the angle where the counterpropagating surface plasmon waves were optimally excited, and the width of the peak is approximately the width of the surface plasmon resonance observed in the attenuated total reflection (ATR) measurement. The theoretical curve in Fig. 7 was calculated from Eq. (33) using Fresnel coefficients deduced from direct fitting of the ATR surface plasmon resonance spectra. Variation of the beam cross-section A with the angle θ was also taken into account. Then, apart from a normalization constant, there was no other adjustable parameter in the theoretical calculation. Figure 7 shows very good agreement between theory and experiment. The slight shift of the theoretical curve relative to the data points can be easily accounted for by a possible 0.2° wedge between the quartz and

prism faces.

Also verified in the experiment was that the generated second harmonic beam was highly directional along the surface normal with a divergence of ~ 1 mrad, and was linearly polarized along $\hat{x}$. It disappeared when one of the counterpropagating laser beams was blocked, or when the laser beam was made transverse electric so that the surface plasmons could no longer be excited, or when the quartz crystal was replaced by a glass substrate. From Eq. (33), the predicted second harmonic output was $\mathscr{P}(2\omega) = 5 \times 10^{-25} \mathscr{P}_1(\omega)\, \mathscr{P}_2(\omega)/A$ in cgs units. Note that because of the relatively poor coupling to the surface plasmon, $R_{MIN} \sim 50\%$, the maximum value of $|\vec{\mathcal{E}}_q|/|\vec{\mathcal{E}}_{inc}|$ was ~ 2.5. In the actual experiment, with $\mathscr{P}_1(\omega) = 3.5 \times 10^{12}$ erg/sec, $\mathscr{P}_2(\omega) = 1.7 \times 10^{12}$ erg/sec and $A \cong 0.25$ cm^2, theoretically, a second harmonic output of 2×10^4 photons/pulse was expected. Taking into account the collection of efficiency of the experimental detection system, the maximum observed signal was $\sim 10^4$ photons/pulse.

The theory also predicts the generation of a second harmonic beam corresponding to $\vec{E}_p$ propagating out along the surface normal from the prism. This beam, in passing through the silver film is attenuated by a factor $e^{-2\alpha_m d}$. However, experimentally, a sizeable background arising from second harmonic generation in the glass prism masked the predicted signal.

In conclusion, the nonlinear interaction of two counterpropagating surface plasmon waves can lead to the generation of a bulk second harmonic wave propagating out from the surface along the surface normal. In terms of language of photons, this would mean that two counterpropagating photons could annihilate one another and create a second harmon-

ic photon propagating in the orthogonal direction. Because the effect was easily observable, it could be used to study second order nonlinear optical properties of thin films.

One of the most interesting cases would be to study $\chi^{(2)}$ of thin metal films, and in particular, thin silver films. Because all metals have inversion symmetry, $\chi^{(2)} = 0$ in the El approximation. The induced second order nonlinear polarization therefore arises from Ml and E2 contributions, and can be written as[25]

$$\vec{P}^{(2)}(2\omega) = \alpha(\nabla \cdot \vec{E})\vec{E} + \beta(\vec{E} \cdot \nabla)\vec{E} + \gamma\vec{E} \times \vec{H} \qquad (34)$$

where the first two terms are electric quadrupole (E2) and the last term is magnetic dipole (Ml). In general, all terms can give rise to bulk as well as surface contributions; however, for a single input wave in isotropic metals, the E2 terms give rise only to a nonlinear surface contribution, and the Ml term gives rise only to a nonlinear bulk contribution. Furthermore, for metals, the E2 terms are nonvanishing only within the Thomas-Fermi screening length,[26] i.e. only the first few atomic layers at the surface, and can be interpreted as an El surface layer lacking inversion symmetry. In the case of second harmonic generation by counterpropagating surface plasmons at a silver-air interface, the corresponding bulk and surface contributions to the nonlinear polarization obtained from Eq. (34) have a vanishing component parallel to the surface (see Appendix); it should be noted that this results strictly from symmetry considerations. Consequently, no second harmonic generation along the surface normal should be observed, and indeed, no such second harmonic signal was observed; only second harmonic

signal corresponding to a single surface plasmon input was observed. Experimentally, the TM input was provided by a doubled Nd:YAG pumped dye laser, at ~ 6328 Å, linewidth ~ 0.3 cm^{-1}, ~ 7 ns pulse length at 10 pulses per second. The experimental set up was similar to that shown in Fig. 6(a), but with a simple prism-silver film-air ATR geometry, and using a 3 cm saturated $NiSO_4$ aqueous solution[27] and a Corning 7-54 color filter to separate the fundamental and second harmonic signals. Approximately 1 mJ of energy in a 5 mm diameter in each counterpropagating beam was incident on the prism-silver interface. Finally, although second harmonic generation for exactly propagating surface plasmons is forbidden by symmetry, by varying the angle between the two fundamental surface plasmons, one should be able to determine the coefficients α, β, and γ of Eq. (34).

C. Coherent Third Harmonic Generation by Surface Plasmons

The next level of complexity in nonlinear interaction of surface plasmons involves third order or $\chi^{(3)}$ processes. Here, experimental results for third harmonic generation will be presented.[28] Using the formalism developed earlier, the experimental results will be shown to be in good agreement with theory. In addition, $\chi^{(3)}(3\omega = \omega + \omega + \omega)$ for methanol will be estimated from the experimentally observed signal.

Consider third harmonic generation by a single surface plasmon input at a silver-organic liquid (methanol) interface. Physically, the input surface plasmon at frequency ω generates $\vec{P}^{NL}$ at 3ω in both the metal and liquid. $\vec{P}^{NL}$ in turn radiates, generating a bulk third harmonic wave which can be detected on the prism side. In practice, the nonlinearity of the liquid dominated the third harmonic generation as

evidenced by the reduction of the third harmonic signal beyond detectibility when the liquid was replaced by air. The surface plasmons along the silver-methanol interface were excited using the Kretschmann configuration, as shown in Fig. 8(a). With the input surface plasmon field given by

$$\vec{E}_{1\ell} = \vec{\mathcal{E}}_{1\ell} e^{ik_{1x}x + \alpha_{1\ell}z} e^{-i\omega t} + \text{c.c.} \qquad z \leq 0 \tag{35}$$

then

$$\vec{P}^{NL} = \chi^{(3)}(3\omega = \omega + \omega + \omega) : \vec{\mathcal{E}}_{1\ell}\vec{\mathcal{E}}_{1\ell}\vec{\mathcal{E}}_{1\ell} e^{i3k_{1x}x - 3\alpha_{1\ell}z} e^{-i3\omega t}$$

$$= \left\{ \frac{i\alpha_{1\ell}\hat{x} + k_{1x}\hat{z}}{k_\ell} \right\} \chi^{(3)}_{1111} |\vec{\mathcal{E}}_{1\ell}|^3 \tag{36}$$

where the subscript ℓ for liquid has replaced subscript d used earlier, $\chi^{(3)}_{1111}$ is the third order nonlinear susceptibility for methanol, and $\vec{\mathcal{E}}_{1\ell}$ is related to the incident fields in the prism by the usual Fresnel coefficient, Eq. (14). To obtain the explicit form of $\vec{P}^{NL}$ in Eq. (36) above, the form of $\chi^{(3)}$ for inversion symmetric media and nonresonant nonlinear generation was used. Using Eq. (29) to calculate $\vec{\mathcal{E}}_p$, the third harmonic field in the prism, the power radiated in the prism given by

$$\mathcal{P}(3\omega) = \frac{c}{2\pi}\sqrt{\epsilon_p}\, A \left| \frac{8\pi\alpha_m k_p \epsilon_m \left(\alpha_\ell \alpha_{1\ell} + 3k_{1x}^2\right) e^{-\alpha_m d} \chi^{(3)}_{1111} |\vec{\mathcal{E}}_{1\ell}|^3}{D(3k_{1x}, 3\omega) k_{1\ell} (3\alpha_{1\ell} + \alpha_\ell)} \right|^2 \tag{37}$$

where ϵ_p, ϵ_m, α_m, and α_ℓ are evaluated at 3ω, and A is the cross sectional area of the input beam.

The experimental set up is shown in Fig. 8(b). A Quanta Ray DCR1A laser provided 20 mJ, 10 nsec, TM 1.06 μm laser pulses in ~ 1 cm^2 beam cross section at 10 pulses per second. The sample cell was mounted on a rotary table, and consisted of methanol in contact with a thin (~ 450 Å) silver film which was evaporated onto an equilateral F2 prism. The input intensity and the efficiency of the surface plasmon excitation were monitored by using beam splitters. The third harmonic signal was detected on the prism side and directed to the monochromator by an angularly adjustable mirror at the exit face of the prism, as shown in Fig. 8(b).

The experimental results are shown in Fig. 9, with the excitation of the surface plasmon and the third harmonic signal plotted as a function of angle of incidence. The maximum of the third harmonic signal occurs, as expected, at the angle of optimum surface plasmon excitation, and the angular width of the signal was less than half the width of the surface plasmon resonance, as theoretically expected. The third harmonic signal was verified to be a narrow band signal at 3ω, highly directional with a beam divergence < 1 mrad, and linearly polarized along $\hat{x}$. Also, when the input polarization was rotated to TE so that surface plasmons could no longer be excited, the signal disappeared as expected. From Eq. (37), the predicted third harmonic output is given by

$$\mathcal{P}(3\omega) = 2.6 \times 10^{-14} |\chi^{(3)}_{1111}|^2 (\mathcal{P}_1(\omega))^3 / A^2 \qquad (38)$$

in cgs units, where $\mathcal{P}_1(\omega) = \frac{c}{2\pi}\sqrt{\epsilon_p}|\vec{\mathcal{E}}_{inc}(\omega)|^2$ is the fundamental power incident at the prism-silver interface. Because $\chi^{(3)}_{1111}(3\omega = \omega + \omega + \omega)$

has not been reported in literature, from the observed signal, Eq. (38) can be used to estimate $\chi^{(3)}$. From the observed signal, ~ 1 photoelectron per pulse, after accounting for the quantum efficiency of the photomultiplier, the throughput efficiency of the monochromator, and the overall collection efficiency, the estimated third harmonic signal generated was $\sim 10^2$ photons/pulse. Thus, using Eq. (38)

$$|\chi^{(3)}_{1111}(3\omega = \omega + \omega + \omega)| \cong 3.0 \times 10^{-14} \text{ esu.} \tag{39}$$

Note that for the convention $\mathcal{P} = \frac{cn}{8\pi}|\vec{\mathcal{E}}|^2$ and $\vec{E} = \frac{1}{2}\vec{\mathcal{E}}e^{ik\cdot r - i\omega t} + \text{c.c.}$, then $|\chi^{(3)}| \cong 7.5 \times 10^{-15}$ esu. Also, in calculating the numerical values in Eqs. (39) and (40), the enhancement factor, $t_{pm\ell}$, was ~ 6, as determined by fitting the experimental reflectivity dip.

As mentioned earlier, in principle one should also be able to observe third harmonic generation in the metal film, with the liquid replaced by air; however, because

$$\frac{|\vec{\mathcal{E}}_m|^2}{|\vec{\mathcal{E}}_{air}|^2} = \frac{1}{|\epsilon_m|} \tag{40}$$

for surface plasmons at a silver-air interface, $\epsilon_m \cong -60$ at 1.06 μm, unless $\chi^{(3)}(3\omega = \omega + \omega + \omega)$ for silver were much larger than for methanol, the signal would be extremely difficult to detect without the use of picosecond lasers.

D. Surface Coherent AntiStokes Raman Spectroscopy

In all cases of harmonic generation by surface plasmons discussed to this point, because of the dielectric function of the metal, $K'_x(3\omega)$

$> 3K_x'(\omega)$ and $K_x'(2\omega) > 2K_x'(\omega)$ and therefore, lacking anomalous dispersion of the dielectric medium, it was impossible to phase match those nonlinear processes. However, in a more general nonlinear process of four wave mixing, it is possible to phase match the nonlinear generation. In particular, for surface coherent antiStokes Raman spectroscopy (CARS), experimental results for a surface nonlinear process, in which all input and output waves are surface plasmons, will be presented,[9] and will be shown to be in good agreement with the theory. In addition, the ultimate sensitivity of the surface CARS technique will be evaluated.

The physical processes giving rise to the nonlinear surface CARS signal can be easily understood. Consider two surface plasmon waves at ω_1 and ω_2 propagating on a plane boundary surface between a metal and dielectric medium with wavevectors $(\vec{k}_1)_{\parallel}$ and $(\vec{k}_2)_{\parallel}$, respectively, parallel to the surface. These waves interact on the surface via the third order nonlinearity in the dielectric medium, producing a third order nonlinear polarization at $\omega_a = 2\omega_1 - \omega_2$ which in turn generates a surface antiStokes plasmon wave at ω_a. Furthermore, the antiStokes generation will be phase matched if $(\vec{k}_a)_{\parallel} = 2(\vec{k}_1)_{\parallel} - (\vec{k}_2)_{\parallel}$, and will be resonantly enhanced if $\omega_1 - \omega_2$ approaches the resonant frequency of some excitation in the dielectric medium. Then, just as surface plasmons can be excited by bulk waves incident on the prism side of an ATR geometry, the antiStokes surface plasmons can couple to bulk waves and be detected on the prism side.

The theory of surface CARS, as derived in Eqs. (26) and (29), is governed by the nonlinear Maxwell equations. The solution for the special case of surface CARS will be presented here for the sake of com-

pleteness. As before, the Kretschmann configuration was used for the excitation of the surface plasmons, as shown in Fig. 10(a). Incoming TM waves,

$$\vec{E}_{pi} = \vec{\mathcal{E}}_{pi} e^{i\vec{k}_{pi}\cdot\vec{r} - i\omega_i t} + \text{c.c.} \ , \ i = 1,2 \tag{41}$$

on the prism side with $k_{\parallel i} \cong K'_{\parallel}(\omega_i)$, linearly excited surface plasmons described by fields,

$$\vec{E}_{\ell i} = \vec{\mathcal{E}}_{\ell i} e^{i(\vec{k}_{\ell i})_{\parallel}\cdot\vec{\rho} + \alpha_{\ell i} z - i\omega_i t} + \text{c c.} \ , \ i = 1,2 \tag{42}$$

in the liquid, with $\vec{\rho}$ in the x-y plane. The nonlinear polarization governing the antiStokes generation is given by

$$\vec{P}_a^{(3)}(\omega_a = 2\omega_1 - \omega_2) = 3\overleftrightarrow{\chi}^{(3)} : \vec{E}_{\ell 1}(\omega_1)\vec{E}_{\ell 1}(\omega_1)\vec{E}^{*}_{\ell 2}(\omega_2) \tag{43}$$

$$\overleftrightarrow{\chi}^{(3)} = \overleftrightarrow{\chi}^{(3)}_{NR} + \overleftrightarrow{\chi}^{(3)}_{R} \frac{\Gamma}{\omega_v - (\omega_1 - \omega_2) - i\Gamma} \tag{44}$$

where the subscripts R and NR refer to the resonant and nonresonant contributions to $\overleftrightarrow{\chi}^{(3)}$,[29] and ω_v is a vibrational frequency of the liquid medium. The solution, using Eq. (29) when the small TE compone. of $\vec{P}_a^{(3)}$ is neglected, yields a coherent antiStokes TM wave on the prism side,

$$\vec{E}_p = \vec{\mathcal{E}}_p e^{i\vec{k}_{pa}\cdot\vec{r} - i\omega_a t} + \text{c.c.} \tag{45}$$

with amplitude

$$|\vec{E}_p| = \left| 8\pi\epsilon_m k_p \alpha_m \frac{\mathscr{B} e^{-\alpha_m d}}{D(k_x, \omega_a)} \right|$$

$$\mathscr{B} = \frac{-i\alpha_\ell p_x^{(3)} + k_x p_z^{(3)}}{2\alpha_{1\ell} + \alpha_{2\ell} + \alpha_\ell} \tag{46}$$

where $k_x = k_{a\|} = |2(\vec{k}_1)_\| - (\vec{k}_2)_\||$, $\alpha_m^2 = k_x^2 - \epsilon_m \frac{\omega_a^2}{c^2}$, and $\alpha_\ell^2 = k_x^2 - \epsilon_\ell \frac{\omega_a^2}{c^2}$. Note that the expression for $\vec{k}_s$ used in Eq. (46) is given by $\vec{k}_s = 2\vec{k}_1 - \vec{k}_2^*$. The antiStokes power output from the prism side is then given by

$$\mathscr{P}(\omega_a) = \frac{c}{2\pi} \sqrt{\epsilon_p} \int dA |\vec{E}_p|^2 \tag{47}$$

where the surface integration is over the beam cross sectional area.

From Eqs. (41) through (47), one can easily see that the anti-Stokes generation should be strongly enhanced if 1) the incoming waves $\vec{E}_1$ and $\vec{E}_2$ excite surface plasmon resonances so that $k_{i\|} = K_{i\|}$, $i = 1,2$; 2) the surface antiStokes generation is phase matched, Fig. 10(b), so that $k_{a\|} = K'_{a\|}$; and 3) $\omega_1 - \omega_2$ approaches the resonance excitation frequency of the liquid medium so that $\overleftrightarrow{\chi}^{(3)}$ is resonantly enhanced.

The experimental arrangement is shown in Fig. 10(c). A Q-switched ruby laser at 6943 Å with a linewidth ≤ 0.5 cm^{-1} delivered 30-nsec and 500-mJ pulses at a repetition rate of 10 pulses/minute. Part of the beam was used as the ω_1 pump beam and the rest was used to pump a dye laser (NK199 in acetone) oscillator and amplifier system to yield a tunable ω_2 beam at $\sim$ 7456 Å with a linewidth ≤ 1 cm^{-1} and an energy of 20 mJ/pulse. The two beams were then directed from the prism side onto the sample, a glass prism-silver film-benzene combination (Fig.

10(a)) sitting on a rotation table. In order to avoid excessive heating and burning of the metal film, only 2.5 mJ/cm^2 from the ω_1 beam and 25 mJ/cm^2 from the ω_2 beam were used in the experiment. The anti-Stokes output from the prism was then collected by the detection system consisting of an interference filter, a monochromator, and an RCA 7265 photomultiplier. For the purpose of signal normalization and monitoring of the Raman resonance, a bulk CARS experiment on benzene was also set up in parallel. The surface plasmon resonances at ω_1 and ω_2 were monitored and their characteristics determined by independent ATR measurements using the above-mentioned lasers.

In order to phase match the surface CARS generation and to simultaneously excite the surface plasmons at ω_1 and ω_2 as the prism sample assembly was rotated, it was necessary to rotate the ω_2 beam out of the plane of incidence defined by the ω_1 beam as shown in Fig. 10(b). The Cartesian components of the wavevectors, $\vec{k}_1$, $\vec{k}_2$ and $\vec{k}_a$, both inside and outside the prism could be conveniently calculated and expressed in terms of polar coordinates at the prism-air and prism-silver interfaces. Furthermore, (1) by placing a mirror mount, with calibrated angular adjustment, at the output side of the prism, (2) by recording the angular positions of the mirror mount necessary to send the ω_1 and ω_2 beams parallel to the axis of the collection optics, and (3) by knowing $\vec{k}_a$ with respect to $\vec{k}_1$ and $\vec{k}_2$ on the prism side, one can then accurately extrapolate to the angular position necessary to direct the antiStokes signal to the detection system.

The experimental results on surface CARS are presented in Figs. 11-13 in comparison with theoretical curves derived from Eq. (46). Figure 11 shows the variation of the antiStokes signal as $(\omega_1 - \omega_2)$

moves through the 992-cm^{-1} vibration resonance in $\chi^{(3)}$ of benzene; in this case, the input beams were properly directed so that both ω_1 and ω_2 surface plasmons were optimally excited and the phase matching condition for surface CARS was satisfied. The theoretical curve describing this resonance peak was calculated by using a resonance linewidth determined from the parallel bulk CARS measurement. The nonresonant contribution to $\chi^{(3)}$ must be included in the calculation in order to obtain a good fit to the experimental data in the wings.[29] Aside from an amplitude normalization constant, no other adjustable parameter was used in the calculation of all the theoretical curves. Each data point in the figures was the result of an average over 10 shots. The error bars on the data points presumably arise from laser mode fluctuations.

When both ω_1 and ω_2 beams were fixed in space and in frequency, but the prism-sample assembly was rotated about the $\hat{y}$-axis, the surface CARS signal varied as a result of changing $\vec{k}_{1\|}$ and $\vec{k}_{2\|}$; first, the resonance excitation conditions of the surface plasmons at ω_1 and ω_2 were changed, and then, the phase mismatch in surface CARS was also varied. The results are shown in Fig. 12. Again, the theoretical curve derived from Eq. (46) gives a good fit to the experimental data. Here, the peak is dominated by the effect due to resonance excitation of the surface plasmons at ω_1 and ω_2. The effect of phase mismatch is of secondary importance in reducing slightly the width of the peak. In the present case, the phase matching peak is expected to be extremely broad because the effective interaction length of surface CARS is limited by the attenuation length $1/K_{\|}''$ of the surface plasmons. In Fig. 13, the results on the surface CARS signal versus $\Delta k_{\|} = |2\vec{k}_{1\|} - \vec{k}_{2\|} - \vec{K}_{a\|}|$ are

shown. In the experiment, $\Delta k_{\parallel}$ was varied by changing the direction of $\vec{k}_{2\parallel}$ through variation of $\hat{k}_2$ while keeping the surface plasmons at ω_1 and ω_2 still optimally excited. Here, relatively large uncertainty in the experimental results came from the fact that for each change of $\Delta k_{\parallel}$, the beams had to be readjusted to optimize the beam overlap on the silver film. The theoretical curve is essentially a Lorentzian in $\Delta k_{\parallel}$, arising from the $|D(k_{a\parallel},\omega_a)|^{-2}$ term in Eq. (46), and agrees well with the experimental results.

The antiStokes signal was found to be highly coherent with < 1 mrad beam divergence and TM as expected. Furthermore, the signal disappeared when the ω_1 input beam was rotated to TE. With phase matching and with surface plasmons at both ω_1 and ω_2 optimally excited, the theory predicts a maximum surface CARS output power

$$\mathscr{P}(\omega_a) = 1.1 \times 10^{-34} \mathscr{P}^2(\omega_1)\mathscr{P}^2(\omega_2)/w^4 \qquad (48)$$

in cgs units, at the resonance peak of $\chi^{(3)}$ where w is the incoming beam waist. In calculating the theoretical expression for $\mathscr{P}(\omega_a)$, enhancement factors of $t_{pm\ell} \cong 6.5$ were used, as determined by fitting the experimental reflectivity scans of the ω_1 and ω_2 lasers. Thus, with $\mathscr{P}(\omega_1) = 1.7 \times 10^{12}$ erg/sec and $\mathscr{P}(\omega_2) = 1.7 \times 10^{13}$ erg/sec, in a 0.2 cm^2 beam cross section 30 nsec pulse, an antiStokes output of 2.5×10^5 photons/pulse was expected. The actual experimentally observed signal from the photomultiplier corresponded to $\sim 2 \times 10^5$ photons/pulse, in good agreement with the prediction. The power dependence of the antiStokes output on $\mathscr{P}(\omega_1)$ and $\mathscr{P}(\omega_2)$ was also experimentally verified over an order of magnitude in signal strength. When either the ω_1 or ω_2

beam was blocked, no signal at ω_a was detected after more than 10 shots, indicating that the signal to background ratio in our experiment was greater than 10^3. Bulk CARS generation in the glass prism could contribute to the background, but in our case, it was 6 orders of magnitude smaller than the surface CARS because of phase mismatch.

To demonstrate that the surface CARS could be used to study liquids other than benzene, the technique was also used to probe the 991 and 1030 cm^{-1} Raman modes of pyridine. In this case, the Kretschmann ATR geometry with prism-silver film-pyridine was used. With both the ω_1 and ω_2 surface plasmons optimally excited, and with the phase matching condition for the antiStokes generation satisfied, the surface CARS signal was monitored as $\omega_1 - \omega_2$ was tuned through the Raman resonances as shown in Figs. 14-15. The theoretical curves were calculated using adjustable amplitudes and literature values for the linewidths. In order to obtain a good fit to the experimental data in the wings, it was necessary not only to include a nonresonant contribution to $\chi^{(3)}$,[29] but also to include the interference terms between the two resonances, so that overall,

$$\overleftrightarrow{\chi}^{(3)} = \overleftrightarrow{\chi}^{(3)}_{NR} + \overleftrightarrow{\chi}^{(3)}_{R1} \frac{\Gamma_1}{\omega_{v1} - (\omega_1 - \omega_2) - i\Gamma_1} + \overleftrightarrow{\chi}^{(3)}_{R2} \frac{\Gamma_2}{\omega_{v2} - (\omega_1 - \omega_2) - i\Gamma_2} \tag{49}$$

Because $\chi^{(3)} \propto \frac{d^2\sigma}{d\Omega d\omega}$ for Raman spectroscopy, the ratio of the surface CARS signal should correspond directly to the Raman scattering cross sections. Experimentally, the ratio of the 991 cm^{-1} to the 1030 cm^{-1} nonlinear signal was ~ 2.5, in good agreement with the square of the experimental ratio of the Raman cross sections, $(1.5)^2 = 2.25$.[30] For an input of 2.8 mJ/cm^2 at ω_1 and 32 mJ/cm^2 at ω_2, with a 30 ns pulse-

width and a beam cross section of 0.25 cm^2, the measured signal at the resonance 991 cm^{-1} peak corresponded to $\sim 1.5 \times 10^4$ photons/pulse, while 3.3×10^4 photons/pulse was theoretically predicted. Furthermore, the surface CARS signal was found to be a highly directional beam, and as expected, was a maximum when the surface plasmons at ω_1 and ω_2 were optimally excited.

Finally, as mentioned earlier, surface plasmons have relatively short attenuation lengths ℓ because of the large ϵ'' in the metal. Typically, $\ell = \frac{1}{K_x''} \sim 10$ μm for a surface plasmon at a silver dielectric interface, with ω in the visible region; thus, the interaction length in surface CARS is ~ 10 μm. Therefore, even if the dielectric medium were to be strongly absorbing, the antiStokes signal would not be expected to be appreciably reduced by the absorption. Experimentally, the surface CARS signal from a 1:2 acetone-benzene mixture on silver was observed and carefully characterized. When 1.1 mM of oxazine 725 was dissolved in the acetone-benzene solution, yielding an absorption coefficient of ~ 400 cm^{-1} at the antiStokes frequency, the surface CARS signal was essentially unchanged, as expected.[28]

In summary, surface CARS is a surface specific probe, and in comparison with bulk CARS has some advantages and rather unique applications. Because the incident laser fields are strongly enhanced, the induced nonlinear polarization is corresponding nonlinearly enhanced, by $(t_{pmd})^6$. Because the effective interation length in surface CARS is only $\frac{1}{K_x''} \sim 10$ μm, the technique can be used to probe $\chi^{(3)}$ for media with strong absorption and fluorescence. Also, because the fields only extend into the dielectric medium a distance $\sim \frac{\lambda}{\pi}$, only a very thin layer of the dielectric medium at the interface effectively contributes to

the surface CARS signal, and the technique can be used to study thin films, overlayers, and perhaps even adsorbed molecules. The sensitivity of the technique with nanosecond laser pulses is limited by optical damage of the metal film. Because the damage for absorbing media usually has an energy fluence rather than an intensity threshold, and because the signal is proportional to $\mathscr{P}^2(\omega_1)\mathscr{P}(\omega_2)$, the ultimate sensitivity of the surface CARS technique could be greatly improved by the use of picosecond pump pulses. In particular, if a 10 psec, 10 μJ/pulse input beams focused to a diameter of 400 μm were used, then, from Eq. (48), the expected surface CARS signal for the prism-silver-benzene system is $\sim 1 \times 10^{11}$ photons/pulse. If there were only a monolayer of benzene molecules on the silver surface, since the signal is proportional to the square of the number of molecules, the expected surface CARS signal would be reduced by 10^4 to 10^5. Thus, the surface CARS technique, with picosecond lasers, should have sufficient sensitivity to detect submonolayers of adsorbed molecules, and because of its surface specific nature, surface CARS should provide a useful tool for applications in surface science.

Chapter IV. Surface Enhanced Second Harmonic Generation at Rough Metal Surfaces

A. Background and Motivation

Since its discovery in 1974,[11] surface enhanced Raman spectroscopy (SERS) has stimulated both experimental and theoretical work on adsorbed molecules at rough metal surfaces.[12] It was found experimentally that the effective Raman cross sections of some molecules adsorbed on rough silver surfaces were 10^5 to 10^6 times larger than those of the same molecules in solution. In this chapter, in an effort to explore and understand this anomalously large enhancement, experimental results as well as a theoretical evaluation of surface enhanced second harmonic generation will be presented.[13] In addition, based on the proposed theoretical model, applications to the detection and spectroscopy of adsorbed molecules will be proposed.

Various mechanisms have been suggested to explain the enhancement. Some involve molecular interaction between the molecules and the metal (known as the chemical effect).[12,31] Others rely on the electromagnetic interaction between molecules and metal (the electromagnetic effect).[12,32] The chemical effect is often the main issue of discussion on SERS, and is evidenced by the observation that only selective molecules on metal surfaces exhibit Raman enhancement.[11] However, it is difficult to understand how an allowed Raman transition of the molecules can have its strength increased by 10^6 through metal-molecule interaction but have its corresponding Raman shift nearly unchanged. The electromagnetic effect, on the other hand, can lead to an enhancement of $\sim 10^4$, as demonstrated by an experiment of Rowe et al.[33] with controlled

surface preparation under ultrahigh vacuum. The local field created by local surface plasmon excitation on the rough surface structure is presumably responsible for the enhancement.[32,34] Most likely, however, it is the combined force of the chemical effect and the electromagnetic effect that gives rise to the total enhancement of $\sim 10^6$. In this respect, it is important to note that in the usual experiments, the minimum observable enhancement factor is $\sim 10^4$ as limited by the sensitivity of the detection system, and the chemical effect may be of critical importance in bringing the total enhancement to a detectable level.

One would like to separate the chemical effect from the electromagnetic effect. This is, unfortunately, very difficult with the molecules adsorbed on the metal surface. However, if the local field enhancement picture is correct then the surface enhanced phenomenon should be rather general. Hartstein et al.[35] have reported an observed enhancement of ~ 20 for infrared absorption of molecular monolayers on metal surfaces. The enhancement should also be present for all nonlinear optical processes. If the metal surface alone has a detectable nonlinearity, then the enhancement of the nonlinear optical effect should be observable on a metal-air interface without the presence of adsorbed molecules. This eliminates the complication of the chemical effect that may change the nonlinear optical coefficient and contribute to the enhancement as in the Raman and infrared cases. Second harmonic (SH) reflection from metal surfaces in air is most interesting.[25] The nonlinearity originates from the first one or two layers of metal atoms at the surface, and according to the theory,[33] the local field enhancement is expected to be strongest in these layers. Here, experimental results on second harmonic reflection (2ω at 0.53 μm) from smooth and

rough surfaces of evaporated films and bulk samples of silver, copper, and gold will be presented.[13] Large enhancements due to surface roughness were actually observed.

B. Local Field Theory

Second harmonic reflection results from the nonlinear polarization $\vec{P}(2\omega)$ induced by the laser on the metal surface,[25]

$$\vec{P}^{(2)}(2\omega) = \alpha(\nabla \cdot \vec{E})\vec{E} + \beta(\vec{E} \cdot \nabla)\vec{E} + \gamma\vec{E} \times (\nabla \times \vec{E}) \tag{50}$$

where α, β, and γ are coefficients characteristic of the metal. Because of the large dielectric constant of a metal, the α and β terms dominate in $\vec{P}^{(2)}(2\omega)$, and are mainly due to contributions from the first one or two layers of metal atoms at the surface. For a rough surface, however, $\vec{P}^{(2)}(2\omega)$ varies over the surface. Intuitively, this local field enhancement can be explained as follows. From electrostatics,[36] the fields at pointed or sharp features on a metal surface can be very large. Furthermore, even if the fields are time varying, as long as the linear dimensions of the sharp features are much less than a wavelength, the results remain valid.

The enhanced fields must result from an accumulation of charge, which can be expressed in terms of a polarization. Furthermore, if one assumes that

$$\vec{E}_{loc}(\omega) = \vec{E}(\omega) + a\vec{P}_L(\omega) \tag{51}$$

and

$$\vec{P}_L(\omega) = b\vec{E}_{loc}(\omega), \tag{52}$$

where a and b are some frequency dependent proportionality constants, then following the usual simple derivation in nonlinear optics,[37]

$$\vec{E}_{loc}(\omega) = L(\omega)\vec{E}(\omega)$$

$$L(\omega) = \frac{1}{1 - ab} \tag{53}$$

and

$$\vec{P}_L^{(2)}(2\omega) \cong \alpha_{eff}(\nabla \cdot \vec{E})\vec{E} + \beta_{eff}(\vec{E} \cdot \nabla)\vec{E} \tag{54}$$

neglecting magnetic-dipole contribution, where $\alpha_{eff} = L^2(\omega)L(2\omega)\alpha$ and $\beta_{eff} = L^2(\omega)L(2\omega)\beta$. McCall et al.[34] showed that for a spheroid,

$$L(\omega) \propto \frac{1}{[\varepsilon(\omega) + 2]} \tag{55}$$

where $\varepsilon(\omega)$ is the dielectric constant of the spheroid. At the surface plasmon resonance of the spheroid, $Re[\varepsilon(\omega) + 2] = 0$ and $L(\omega)$ becomes resonantly enhanced with the enhancement inversely proportional to $Im(\varepsilon)$. For a different geometrical shape of small metal aggregates, $\varepsilon(\omega) + 2$ should be replaced by another function $f(\varepsilon)$, and the surface plasmon resonance is excited when $Re[f(\varepsilon)] = 0$.[38]

The second harmonic signal from reflection is proportional to $\int|\vec{P}_L^{(2)}(2\omega)|^2 dA$, where the integration is over the surface irradiated by the incoming laser beam. The second harmonic generation should be

dominated by $\vec{P}_L^{(2)}(2\omega)$ in regions with the near maximum local field correction. Let x by the fractional area of such regions. Then, the local field enhancement of second harmonic generation from a rough surface over that from a smooth surface should be given approximately by

$$\eta = |L^2(\omega)L(2\omega)|^2_{max} x. \tag{56}$$

C. Experimental Results and Discussion

The experimental setup is shown in Fig. 16. A Q-switched Nd:YAG laser with 10 pulses/sec was used to provide the pump beam at 1.06 μm at a 45° angle of incidence. To avoid damage of the sample surface, the 10 ns pump pulse energy was limited to ~ 7 mJ in a 5-mm diameter spot on the sample. Two types of samples were mainly used in the experiment: smooth evaporated films, ~ 1000 Å thick, and bulk samples roughened by electrolytic cycling. In preparing a rough sample surface, the electrolytic process was performed in 0.1 M KCℓ in water, and with ~ 65 mC/cm^2 of charge transportation occuring in each cycle. As a calibration, we checked that when .05 M of pyridine was also dissolved in the solution, the sample surface obtained after one or two such cycles produced a surface Raman enhancement of ~ 10^6. The roughened sample was taken out of the electrolytic solution (without pyridine), rinsed with distilled water, and finally dried by nitrogen gas before the measurement.

With the sample in the setup shown in Fig. 16, the reflected SH signals (verified to be originating from the Ag sample) were measured and analyzed. In the experiment, it is believed that the second harmonic signal originated from the silver surface for the following rea-

sons. First, any adsorbed molecules present would have been blown off the surface by the first few laser pulses, as this is a well known technique for cleaning surfaces. Second, even if there were a few adsorbed molecules still present, their contribution to the SH signal would be negligible.[25] Third, typically 99.8% of the charge transferred during an electrolytic cycle is recovered,[11] indicating that the residual silver chloride would be much less than a monolayer. Furthermore, enhanced SH signals were already observed from thin silver films evaporated at ~ 100 Å/sec, and from mechanically polished bulk silver samples, neither of which had been exposed to the electrolytic solution. With the 1.06 μm TM input, the signal from the smooth film was a well collimated beam in the specularly reflected direction, and was polarized in the TM mode.[25] The SH signal from the rough surface, however, was highly diffuse, nearly isotropic in angular distribution, as shown in Fig. 17, and independent of both input and output polarizations.

The spectra of the output signals were also analyzed, as shown in Fig. 18 for silver. The second harmonic generation was evidenced by the sharp peak at the second harmonic frequency. In addition, a broad spectral background, highly diffuse and extending from ~ 3500 Å to the infrared (limited to ~ 6000 Å by our detection system), also appeared. For the smooth film, the background was weak, but for the rough surface, it was exceptionally strong.

The second harmonic signal from the electrolytically roughened surface of bulk silver, integrated over the 2π emission solid angle, was found to be 1×10^4 times larger than the collimated SH from the smooth film. The exact value depended somewhat on the surface preparation, but with the same surface preparation procedure, the result was

reproducible to within 20%. Unlike the Raman case, the signal was detectable even from the smooth film, and therefore the enhancement factor was obtained from a direct comparison of two signals, and should be quite accurate except for a possible error of ~ 50% in the measured angular distribution of the diffuse signal from the rough surface. With less electrolytic cycling (less than 65 mC/cm^2), both the second harmonic and the background output became weaker, indicating that roughness was essential for the observed background and signal enhancement.

The laser power dependency of the second harmonic signals from the smooth and rough surfaces was also measured. In all cases, the SH signal was quadratic in laser power, as shown in Fig. 19. For the electrolytically cycled bulk silver samples, the power dependency of the broadband background was found to be $\sim I(\omega)^3$ on the antiStokes side and between $I(\omega)^2$ and $I(\omega)^3$ on the Stokes side, and the pulse shape closely resembled the pump laser pulse. However, for the electrolytically cycled silver films (charge transportation $\lesssim$ 25 mC/cm^2), the power dependency of the broadband background was found to be $\sim I(\omega)^6$ on the anti-Stokes side and $\sim I(\omega)^3$ on the Stokes side. Furthermore, the temporal behavior of the rough film background showed a clear tail, several pulsewidths long. A possible explanation of the different power dependencies could be the different thermal properties of the bulk and thin film samples. From a strictly classical viewpoint, in the bulk silver sample, the maximum rise in temperature due to absorption and subsequent diffusion of energy is expected to be $\lesssim 1°C$.[39] On the other hand, for the thin film, because the thermal conductivity of the substrate (a glass slide) compared to silver is small, the average rise in the temperature, estimated from the total absorbed energy and heat capacity of

silver, is expected to be ~ 20°C; however, locally, the temperature rise may be much larger. Thus, if the antiStokes background arises from phonon assisted processes, a much stronger power dependence would be expected for the case in which there were more thermally excited phonons. Regardless of the detailed mechanism, the results indicate that the broadband background is of luminescence origin. Broadband luminescence from rough surfaces has also been observed with linear excitation in Raman studies.[40]

Similar results were obtained for gold, although both the second harmonic signal and the luminescence background from the rough surface was much weaker. The observed enhancement for second harmonic generation at the electrolytically cycled surface was ~ 10^3. For copper, the broadband luminescence from the rough surface was several times stronger than in silver, and masked off the narrow-band second harmonic signal. Consequently, the surface enhancement for SH on copper, if any, was less than 5×10^3.

Electron micrographs of electrolytically cycled silver surfaces have indicated that the surface roughness consists of ~ 500 Å Ag particles separated by 1500–3000 Å.[33] One can therefore reasonably assume in Eq. (56) the fractional area x where $L(\omega)$ is nearly a maximum due to plasmon resonance to be ~ 5%, and since 2ω is far away from ω in our case, $L(2\omega) \sim 1$. Using the observed enhancement of $\eta = 10^4$ in Eq. (56), $L(\omega) \approx 20$. This value of local field correction is certainly very reasonable considering that on a smooth silver-air interface, the field enhancement due to surface plasmon excitation can already be as high as ~ 20. Copper and gold are expected to have smaller $L(\omega)$ because of the larger values in their $\mathrm{Im}(\varepsilon(\omega))$.

Additional valuable information on the local field enhancement could be obtained by measuring the frequency dependence of the enhanced second harmonic on rough metal surfaces. Furthermore, to obtain a more quantitative comparison between theory and experiment, it would be highly desirable to perform the experiment on a well defined rough surface structure, such as arrays of ellipsoids of the same size formed by lithographic techniques.[38,41] Because the second harmonic signal arises in the first one or two monolayers of the metal atoms, the addition of a layer of adsorbed molecules might significantly increase the second harmonic signal. In particular, techniques for depositing monolayers of organic molecules such as pyridine or benzoic acid, are well known. In attempting to observe the signal from adsorbed molecules, it may be necessary to reduce the laser intensity to prevent the desorption of the adsorbed monolayer. If the second harmonic signal arising from the additional layer is easily observable, it should also be observable on smooth surfaces, and other $\chi^{(2)}$ processes should also be readily observable. In particular, a very interesting application would be sum frequency generation by molecular monolayers. By tuning one of the input frequencies through infrared absorptions, the technique would provide a high resolution surface sensitive infrared probe.

In summary, experimental results from second harmonic generation in reflection from metal surfaces have unambiguously demonstrated that the local fields on rough surface structures can lead to a large enhancement in the strength of a nonlinear optical process. Unlike the Raman case, the metal-molecule interaction does not play a role. In addition, an unusually broad luminescence has been observed from the rough metal surfaces. The mechanism leading to such luminescence is

not yet understood.

Chapter V. Summary and Conclusions

In Chapter II, the linear properties and characteristics of surface plasmons were reviewed. Detailed calculation of the dispersion relation, fields, and Poynting vector were presented. The mathematical formalism of the linear ATR technique to excite surface plasmons was reviewed, in conjunction with simple physical arguments and intuitive interpretations of the results. Realistic numbers characteristic of surface plasmons at silver-dielectric interfaces, based on experimentally obtained data, were calculated, and a detailed description of an experimental setup used to monitor surface plasmon excitation was discussed.

In Chapter III, drawing upon the results of the previous chapter, a detailed theory for nonlinear interaction of surface plasmons was presented. The theory was then used to interpret experimental results for both second and third order nonlinear processes. In particular, results on counterpropagating surface plasmons at a silver-crystal quartz interface generating second harmonic photons propagating normal to the interface were presented. Although symmetry considerations prevented a similar signal from a silver-air interface, an experiment for measuring the E2 and M1 contributions to the nonlinearity of silver was proposed. From experimental results on third harmonic generation by surface plasmons at a silver-methanol interface, a value for $\chi^{(3)}_{1111}(3\omega = \omega + \omega + \omega)$ for methanol was obtained. Results on surface CARS, a surface nonlinear process in which all inputs and outputs are surface plasmons were given. Experimental results for surface CARS at both silver-benzene and silver-pyridine interfaces were presented. Further-

more, the utility of the technique in absorbing media was demonstrated. Based on the experimental results, an ultimate monolayer or even submonolayer detection of adsorbed molecules by the surface CARS technique was predicted.

In Chapter IV, emphasis was shifted to nonlinear interaction at rough metal surfaces. A brief description of the experimental results and numerous theories on surface enhanced Raman spectroscopy provided the motivating force for surface enhanced second harmonic generation. Experimental results for the surface enhanced SH signal were presented and interpreted in terms of a simple local field correction theory. In addition, proposals for further experiments to confirm the local field theory were made. Also, the possibility of using surface enhanced processes to probe adsorbed molecules was proposed.

In conclusion, theories and experimental results for nonlinear interaction at metal-dielectric interfaces have been presented. In the case of nonlinear surface plasmon interaction, the experimental results have verified the theoretical predictions. In addition, because of its surface specific nature and short propagation length, the nonlinear surface plasmon technique can provide very high resolution surface probe, sensitive to changes resulting from adsorbed molecules. With picosecond lasers, the technique could be used for time resolved surface studies, as well as for monolayer detection of adsorbed molecules. Also, the surface plasmon technique can be used to probe more general four wave mixing processes, for example phase conjugation or resonant surface CARS. On the other hand, the experimental results for surface enhanced second harmonic generation have clearly established the importance of the local field correction for light-matter interaction at

rough surfaces. Furthermore, because of the completely general nature of the local field enhancement, it should find important applications in surface science, both in studying general nonlinear processes, and in probing metal-molecule interaction.

References

1. See, for example, a comprehensive review, G. Borstel and H. J. Falge, Appl. Phys. 16, 211 (1978), and references therein.
2. C. F. Eagen and W. H. Weber, Phys. Rev. B 19, 5068 (1979); W. H. Weber, Phys. Rev. Lett. 39, 153 (1977).
3. J. G. Gordon II and J. D. Swalen, Opt. Comm. 22, 374 (1977).
4. V. M. Agranovich, Pis'ma Zh. Eksp. Teor. Fiz. 24, 602 (1976)[JETP Lett. 24, 558 (1976)]; K. C. Chu, C. K. Chen, and Y. R. Shen, Mol. Cryst. Liq. Cryst. 59, 97 (1980).
5. H. J. Simon, D. E. Mitchell, and J. G. Watson, Phys. Rev. Lett. 33, 1531 (1974).
6. H. J. Simon, R. E. Benner, and J. G. Rako, Opt. Comm. 23, 245 (1977).
7. F. DeMartini, M. Colocci, S. E. Kohn, and Y. R. Shen, Phys. Rev. Lett. 38, 1223 (1977).
8. F. DeMartini, G. Guiliani, P. Mataloni, E. Palange, and Y. R. Shen, Phys. Rev. Lett. 37, 440 (1976).
9. C. K. Chen, A. R. B. de Castro, Y. R. Shen, and F. DeMartini, Phys. Rev. Lett. 43, 946 (1979).
10. C. K. Chen, A. R. B. de Castro, and Y. R. Shen, Opt. Lett. 4, 393 (1979).
11. D. L. Jeanmaire and R. P. VanDuyne, J. Elec. Chem. 84, 1 (1977); M. Fleischmann, P. J. Hendra, and A. J. McQuillan, Chem. Phys. Lett. 26, 163 (1974).
12. See, for example, for a review, T. E. Furtak and J. Reyes, Surf. Sci. 93, 351 (1980), and references therein.

13. C. K. Chen, A. R. B. de Castro, and Y. R. Shen, submitted to Phys. Rev. Lett.; Y. R. Shen, C. K. Chen, and A. R. B. de Castro, Proceedings of the Sergio Porto Memorial Symposium on Lasers and Applications, June 29-July 3, 1980, Rio de Janiero.

14. N. M. Chao, K. C. Chu, and Y. R. Shen, submitted to Mol. Cryst. Liq. Cryst.

15. A. Sommerfeld, Ann. Physik 28, 665 (1909).

16. A. Otto, Z. Phys. 216, 398 (1968).

17. E. Kretschmann, Z. Phys. 241, 313 (1971).

18. See, for example, H. Wolter in Handbuch der Physik, S. Flügge, ed. Bd. XXIV (Springer-Verlag, Berlin, 1956), p. 461.

19. For ε_m for silver, copper, and gold, see P. B. Johnson and R. W. Christy, Phys. Rev. B. 6, 4370 (1972); the actual value of ε_m'' varies widely in evaporated films, and should be determined from theoretical fits of the experimental reflectivity curves.

20. F. DeMartini and Y. R. Shen, Phys. Rev. Lett. 36, 216 (1976).

21. N. Bloembergen and P. S. Pershan, Phys. Rev. 128, 606 (1962).

22. M. Fukui, J. E. Sipe, V. C. Y. So, and G. I. Stegeman, Solid State Comm. 27, 1265 (1978); R. Maddox and D. L. Mills, Dept. of Physics, Univ. of Calif., Irvine, Calif. 92717, unpublished.

23. N. Bloembergen, H. J. Simon, and C. H. Lee, Phys. Rev. 181, 1261 (1969).

24. R. Normandin and G. I. Stegeman, Opt. Lett. 4, 58 (1979).

25. N. Bloembergen, R. K. Chang, S. S. Jha, and C. H. Lee, Phys. Rev. 174, 813 (1968).

26. C. S. Wang, J. M. Chen, and J. R. Bower, Opt. Comm. 8, 275 (1973).

27. M. Kasha. J. Opt. Soc. Amer. 38, 929 (1948).

28. Results were reported by C. K. Chen, A. R. B. de Castro, and Y. R. Shen, XI Internatl. Quant. Elec. Conf., Boston, June 23-26, 1980, paper N7.

29. J. J. Song and M. D. Levenson, J. Appl. Phys. 48, 3496 (1977).

30. See, for example, the Raman spectrum of pyridine published in M. Fleischmann et al. of Ref. 11.

31. See, for example. A. Otto, J. Timper, J. Billman, and I. Pockrand, Phys. Rev. Lett. 45, 46 (1980); J. I. Gersten, R. L. Birke, and J. R. Lombardi, Phys. Rev. Lett. 43, 147 (1979); E. Burstein, Y. J. Chen, C. Y. Chen, S. Lundquist, and E. Tosatti, Solid State Comm. 29, 567 (1979); S. S. Jha, J. R. Kirtley, and J. C. Tsang, Phys. Rev. B (to be published).

32. See, for example, D. A. Weitz, T. J. Gramila, A. Z. Genack, and J. I. Gersten, Phys. Rev. Lett. 45, 355 (1980); M. Moskovitz, J. Chem. Phys. 69, 4159 (1978); G. L. Eesley and J. R. Smith, Solid State Comm. 31, 815 (1979).

33. J. E. Rowe, C. V. Shank, D. A. Zwemer, and C. A. Murray, Phys. Rev. Lett. 44, 1770 (1980).

34. S. L. McCall, P. M. Platzman, and P. A. Wolff, Phys. Lett. 77A, 331 (1980).

35. A. Hartstein, J. R. Kirtley, and J. C. Tsang, Phys. Rev. Lett. 45, 201 (1980).

36. J. D. Jackson, Classical Electrodynamics, 2nd edition (Wiley, 1975) p. 78.

37. N. Bloembergen, Nonlinear Optics (W. A. Benjamin, 1977) p. 68.

38. For a theoretical calculation of SERS resulting from an array of ellipsoids, see C. Y. Chen and E. Burstein, Phys. Rev. Lett. 45,

1287 (1980).

39. B. F. Levine, C. V. Shank, J. P. Heritage, IEEE, J. Quant. Elec. QE-15, 1418 (1979).

40. R. L. Birke, J. R. Lombardi, and J. I. Gersten, Phys. Rev. Lett. 43, 71 (1979); J. P. Heritage, J. G. Bergman, A. Pinczuk, and J. M. Worlock, Chem. Phys. Lett. 67, 229 (1979).

41. P. F. Liao, U.S.-Japan Bilateral Seminar on Nonlinear Laser Spectrsocopy, Sept. 8-12, Kauai, Hawaii.

Figure Captions

Fig. 1 Schematic of a surface electromagnetic wave propagating along $\hat{x}$. The amplitude of exponentially decaying fields is plotted versus z.

Fig. 2 Surface plasmon dispersion curve for a metal-dielectric interface.

Fig. 3 The Kretschmann ATR configuration.

Fig. 4 Reflectivity versus the angle of incidence θ, defined in Fig. 3, showing the sharp dip resulting from surface plasmon excitation. The solid curve is a theoretical curve that fits the experimental data points (after Ref. 4, K. C. Chu et al.).

Fig. 5 Experimental setup used to monitor surface plasmon excitation.

Fig. 6 (a) The sample assembly.

(b) Block diagram of the experimental setup. F is a 10 cm long cell with an aqueous solution of saturated $CuSO_4$.

Fig. 7 Second harmonic intensity versus θ. θ is defined in Fig. 6(a).

Fig. 8 (a) The sample assembly.

(b) Schematic of the experimental setup.

Fig. 9 (a) Reflectivity of the incident laser beam versus θ. θ is defined in Fig. 8(a).

(b) Third harmonic intensity versus θ.

Fig. 10 (a) Prism-metal-liquid assembly. Beam 1 propagates in the x-z plane, beam 2 and the output do not.

(b) Wavevectors in the glass prism; components in the x-y plane are phasematched.

(c) Block diagram of the experimental setup. IF is an inter-

ference filter and L is a lens.

Fig. 11 Surface CARS signal (benzene) versus $(\omega_1 - \omega_2)$ near resonance.

Fig. 12 Surface CARS signal (benzene) versus the angular position of the prism assembly about the $\hat{y}$ axis. θ is the angle between the direction of beam 1 incident on the prism and the prism normal.

Fig. 13 Surface CARS signal (benzene) versus the phase mismatch, $(\Delta k)_{\parallel}$.

Fig. 14 Surface CARS signal (pyridine) versus $(\omega_1 - \omega_2)$ near the 991 cm^{-1} Raman resonance.

Fig. 15 Surface CARS signal (pyridine) versus $(\omega_1 - \omega_2)$ near the 1030 cm^{-1} Raman resonance.

Fig. 16 Experimental setup; F1 is a red cutoff filter, F2 is an infrared blocking, visible passing color filter, IF is a narrowband interference filter, center wavelength 0.53 μm, and L is a f/1 collection lens.

Fig. 17 Angular distribution of the surface enhanced second harmonic signal, from rough bulk silver, in the plane of incidence.

Fig. 18 Spectral distribution of the nonlinear signal from a rough bulk silver sample.

Fig. 19 Power dependencies of the nonlinear signal on silver; the upper and lower curves show the quadratic dependency of the diffuse SH signal from the rough bulk sample and of the collimated SH signal from the smooth film, respectively; the dashed curve shows the cubic dependency of the diffuse antiStokes signal from the rough bulk sample.

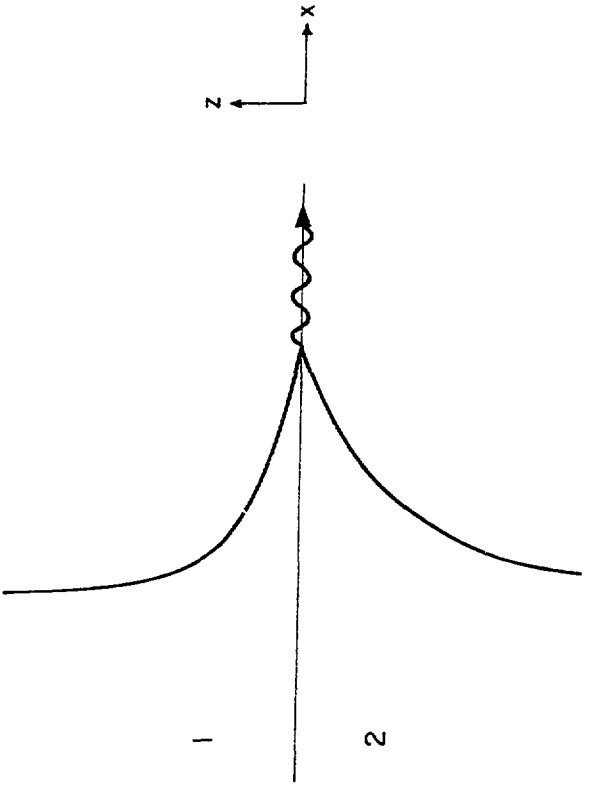

XBL8011-6279

Fig. 1

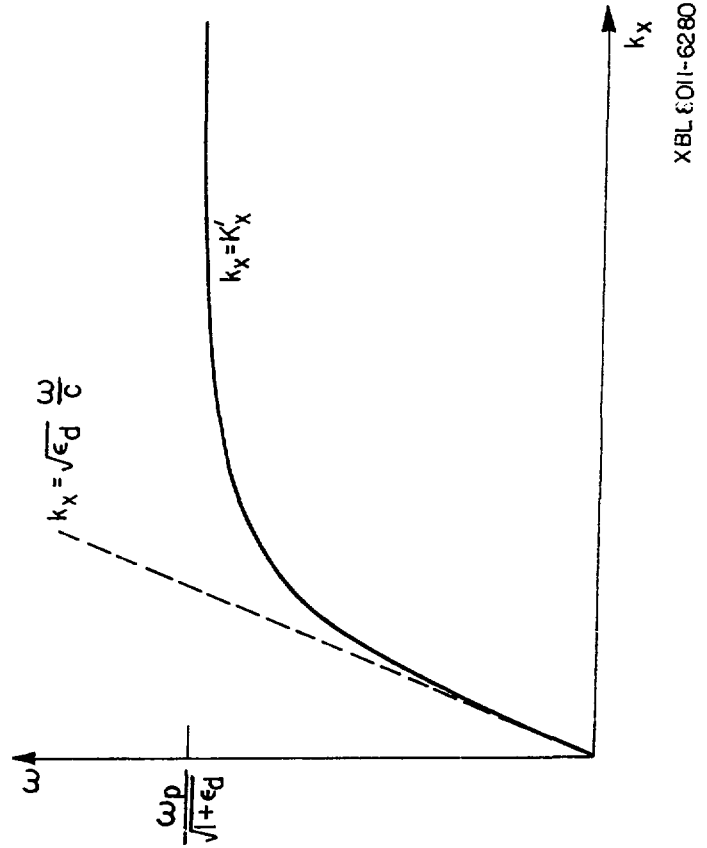
$k_x = \sqrt{\epsilon_d}\,\omega/c$
$k_x = K'_x$
ω
$\frac{\omega_p}{\sqrt{1+\epsilon_d}}$
k_x
XBL 8011-6280

Fig. 2

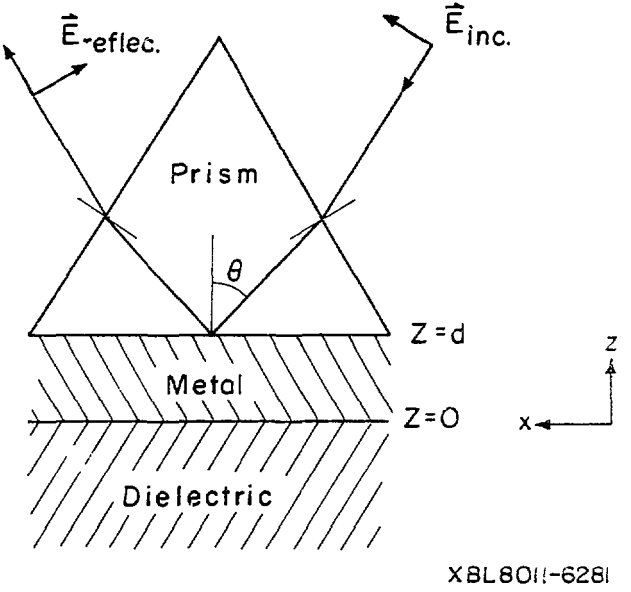
$\vec{E}_{reflec.}$
$\vec{E}_{inc.}$
Prism
θ
Z=d
Metal
Z=O
Dielectric
z
x
XBL801-6281

Fig. 3

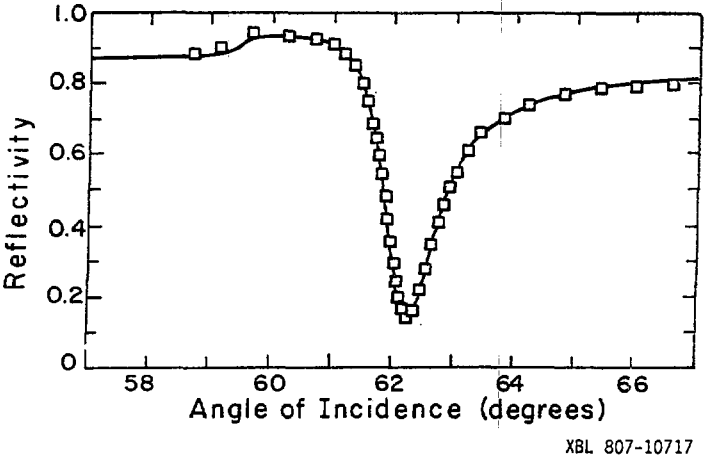
1.0
0.8
0.6
0.4
0.2
0
Reflectivity
58
60
62
64
66
Angle of Incidence (degrees)
XBL 807-10717

Fig. 4

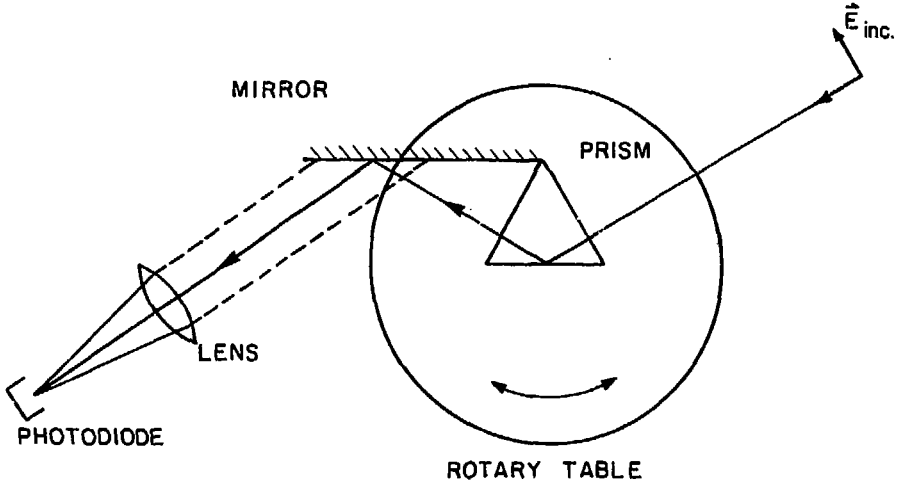

XBL 8011-6282

Fig. 5

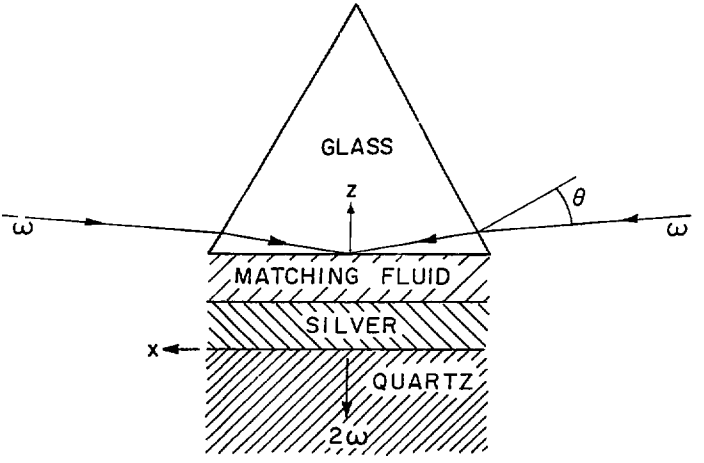

(a)

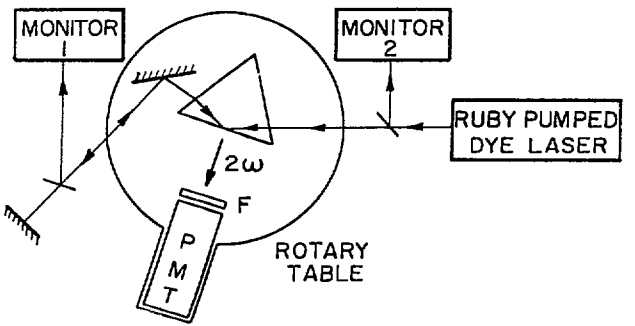

(b)

XBL797-6702

Fig. 6

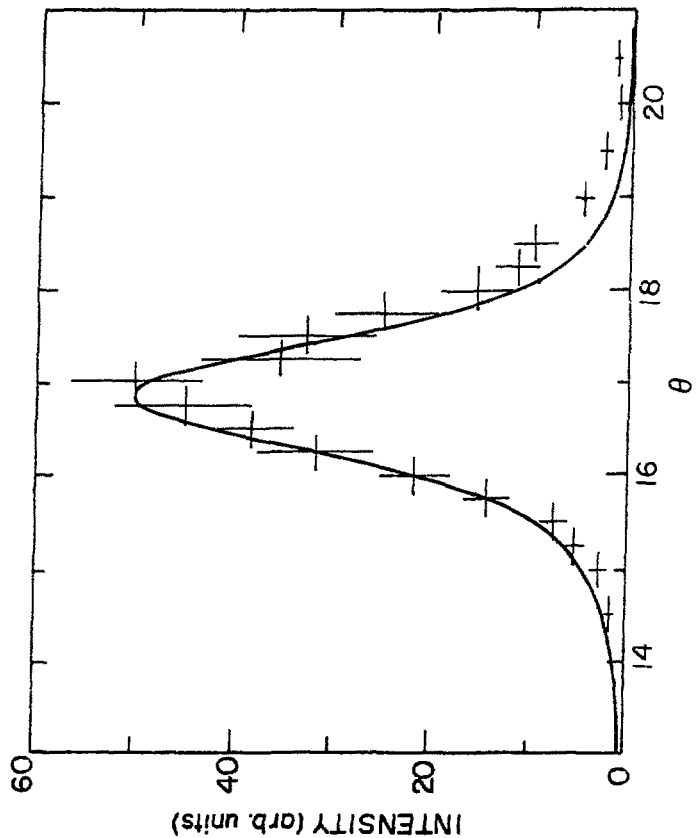

XBL797-6701

Fig. 7

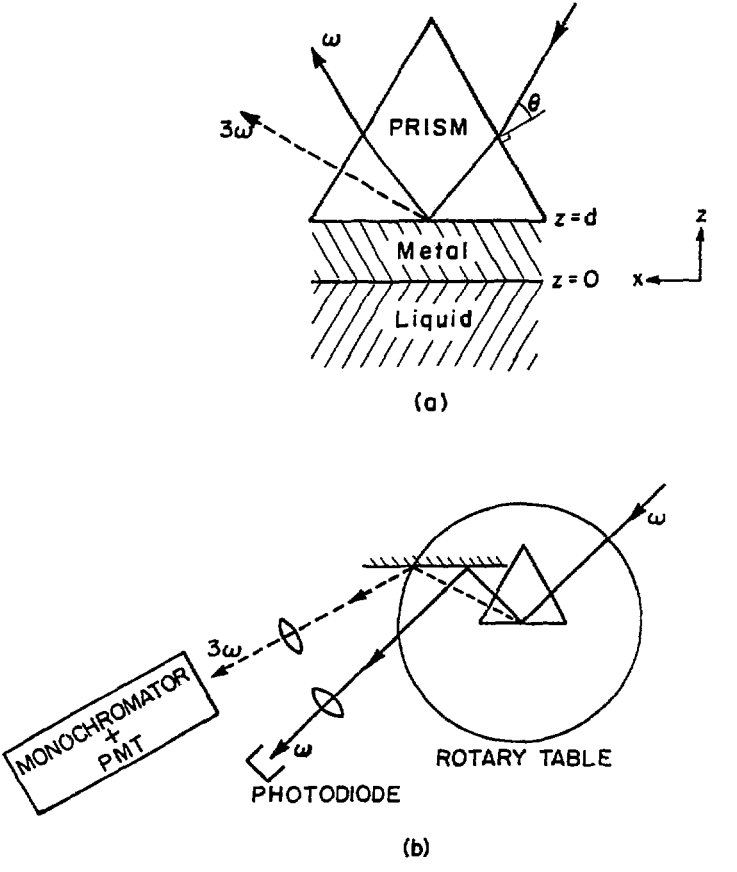
ω
3ω
PRISM
θ
z=d
Metal
z=0
Liquid
z
x
(a)
ω
3ω
MONOCHROMATOR
+
PMT
ω
ROTARY TABLE
PHOTODIODE
(b)
XBL 8011-6283

Fig. 8

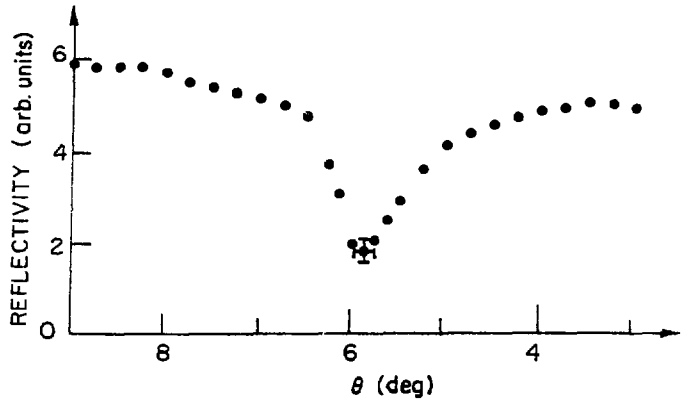

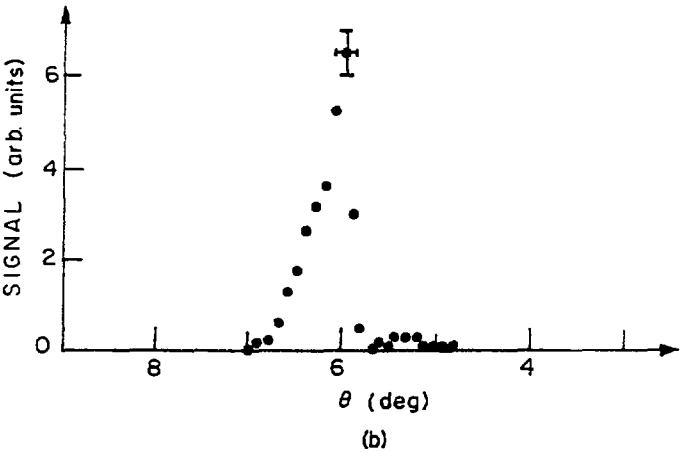

XBL 8011-6284

Fig. 9

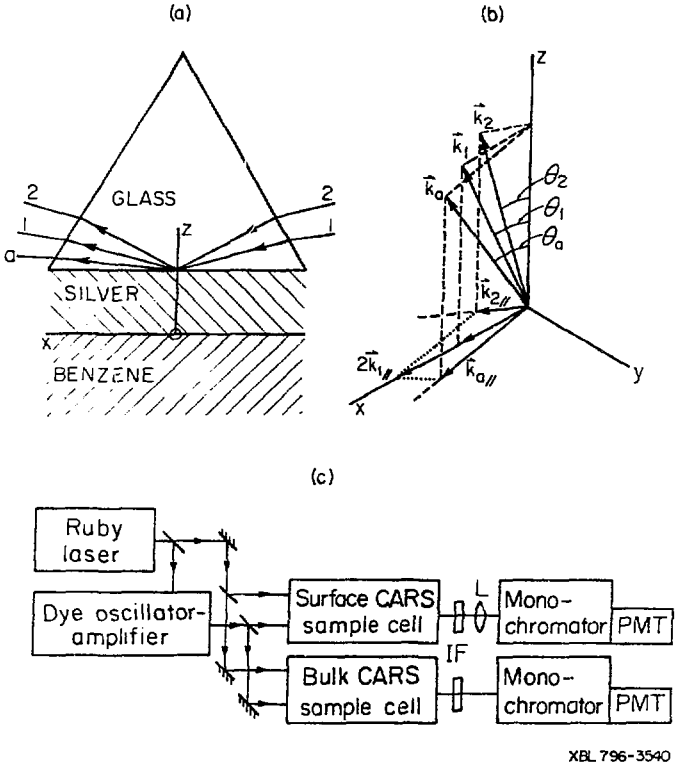
(a)
(b)
(c)
GLASS
SILVER
BENZENE
Ruby laser
Dye oscillator-amplifier
Surface CARS sample cell
Bulk CARS sample cell
L
IF
Mono-chromator
PMT
Mono-chromator
PMT
XBL 796-3540

Fig. 10

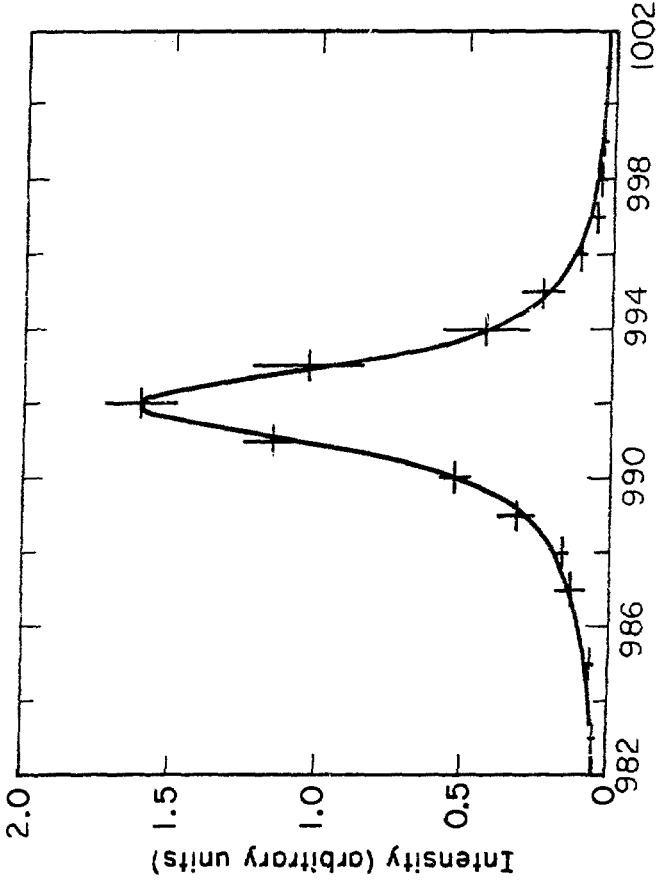

XBL796-3537

Fig. 11

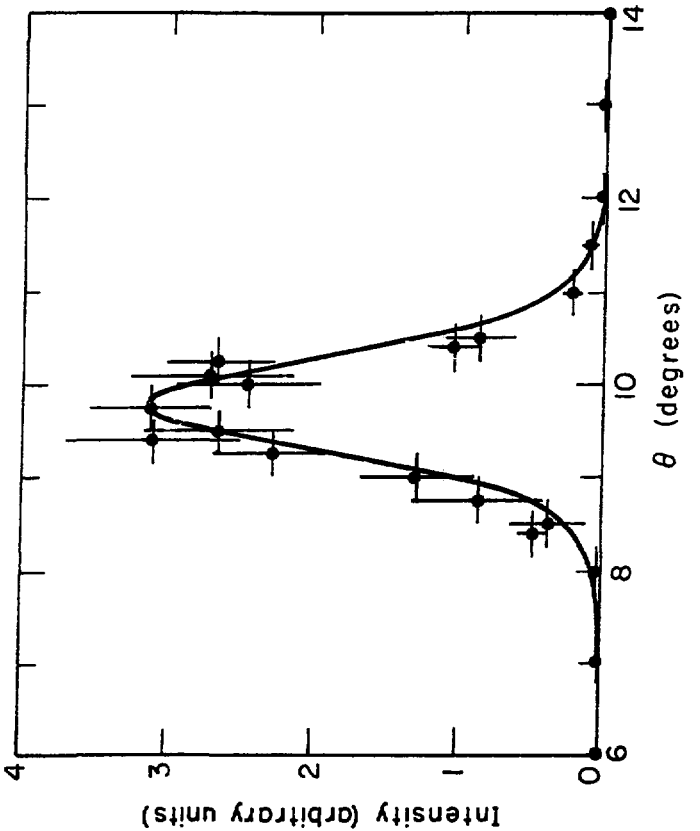

XBL796-3539

Fig. 12

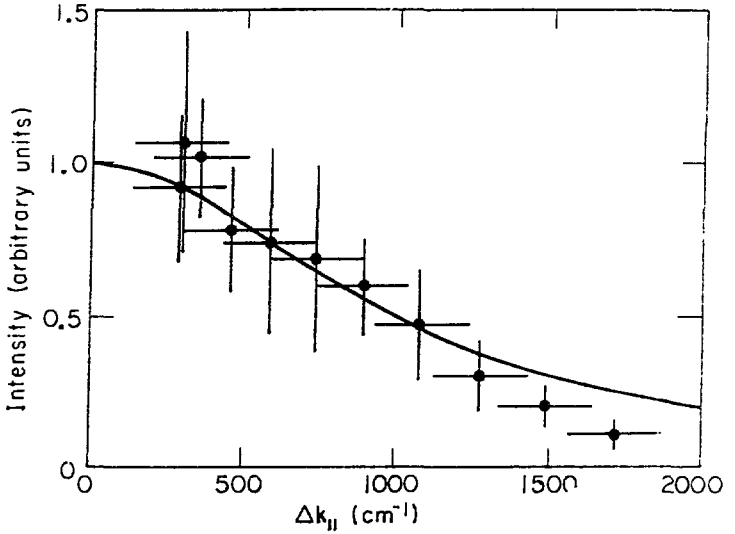
1.5
1.0
0.5
0
0
500
1000
1500
2000
Intensity (arbitrary units)
$\Delta k_{\parallel}$ (cm^{-1})
XBL796-3538

Fig. 13

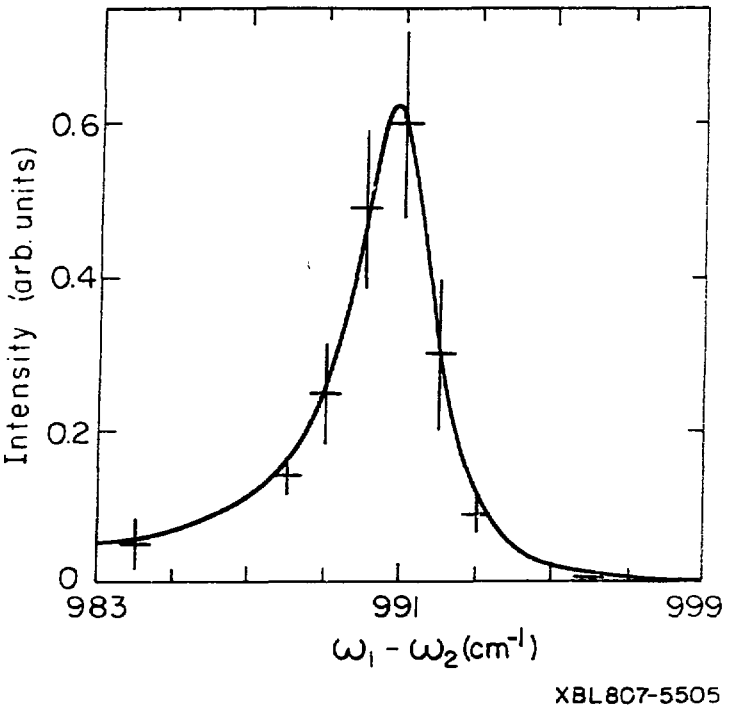
Intensity (arb. units)
0.6
0.4
0.2
0
983
991
999
$\omega_1 - \omega_2 (cm^{-1})$
XBL807-5505

Fig. 14

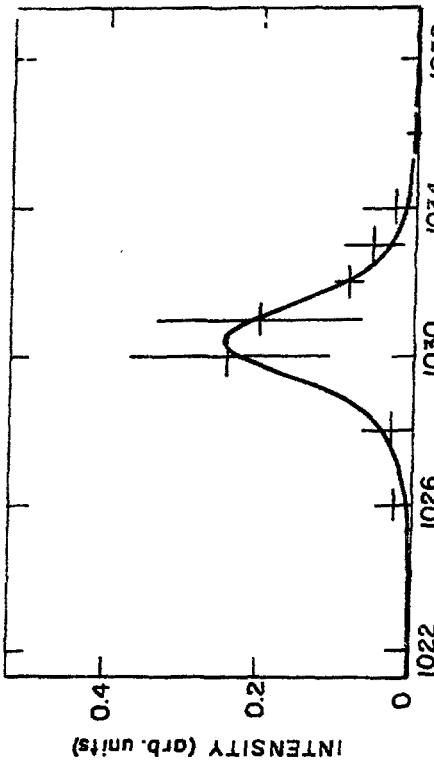
INTENSITY (arb. units)
0
0.2
0.4
1022
1026
1030
1034
1038
$(\omega_1-\omega_2)$ (cm^{-1})
XBL 8011-6285

Fig. 15

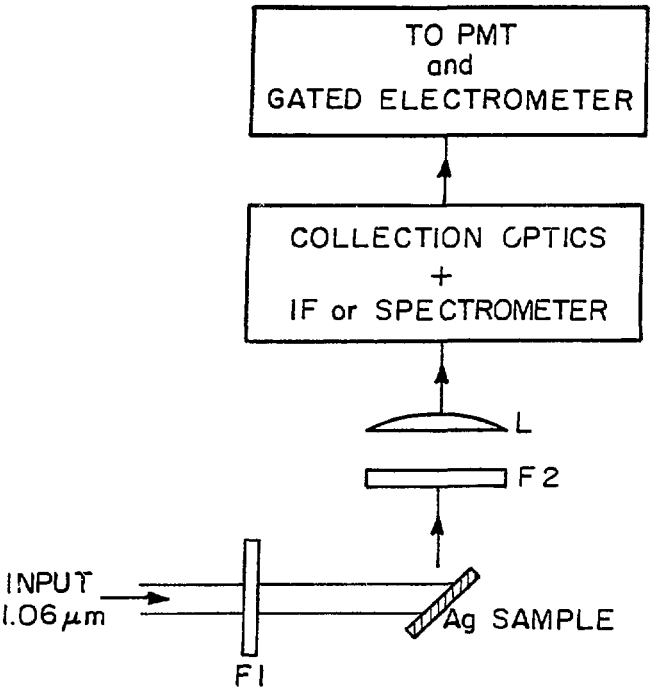
TO PMT
and
GATED ELECTROMETER
COLLECTION OPTICS
+
IF or SPECTROMETER
L
F2
INPUT
1.06 μm
Ag SAMPLE
F1
XBL809-5839

Fig. 16

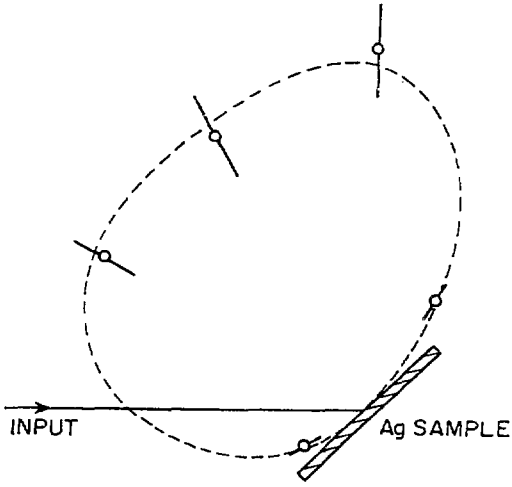

XBL 809-5842

Fig. 17

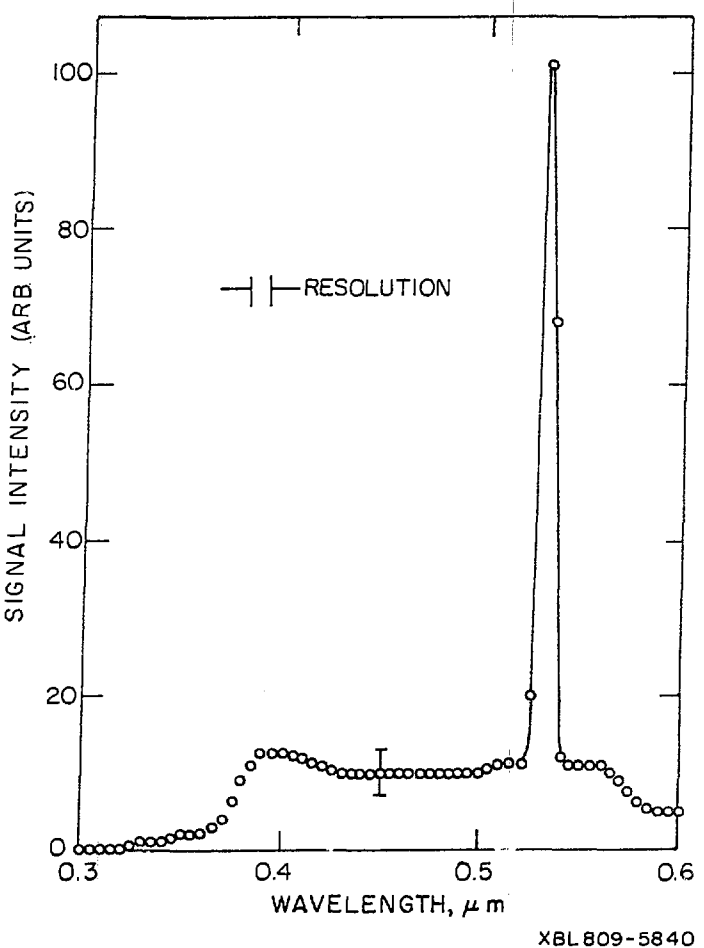
100
80
60
40
20
0
SIGNAL INTENSITY (ARB. UNITS)
RESOLUTION
0.3
0.4
0.5
0.6
WAVELENGTH, μm
XBL809-5840

Fig. 18

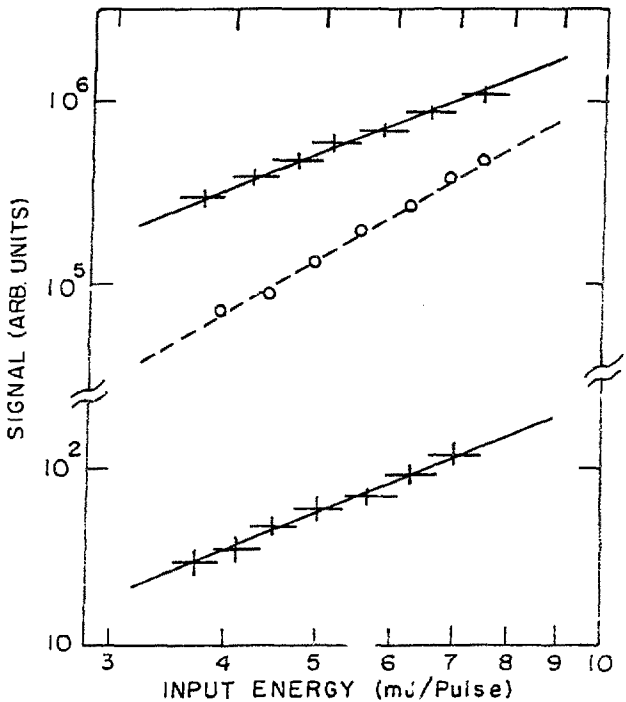
SIGNAL (ARB. UNITS)
10^6
10^5
10^2
10
3
4
5
6
7
8
9
10
INPUT ENERGY (mJ/Pulse)
XBL 809-5841

Fig. 19

Appendix. Bulk and Surface Contributions to $\vec{P}^{(2)}$ for Counterpropagating Surface Plasmons

In the appendix, the general form of $\vec{P}^{(2)}$ for inversion symmetric media, including both the bulk and the surface contributions, will be explicitly evaluated for the case of counterpropagating surface plasmons at a metal-air interface. In this case, it will be shown that $\vec{P}^{(2)}$ has a nonzero component only normal to the surface, along $\hat{z}$, and thus cannot radiate a coherent second harmonic beam propagating along $\hat{z}$.

Consider surface plasmons propagating along $\pm \hat{x}$ at a metal ($z \geq 0$) -air ($z \leq 0$) interface. The induced second order nonlinear polarization arises from E2 and M1 contributions in the metal, and can be written as[25]

$$\vec{P}^{(2)} = \alpha(\nabla \cdot \vec{E})\vec{E} + \beta(\vec{E} \cdot \vec{\nabla})\vec{E} + \gamma\vec{E} \times \vec{H}. \tag{A1}$$

Drawing from the results of Chapter II, the input fields in the metal for counterpropagating surface plasmons are given by

$$\vec{\mathcal{E}}_1 = \mathcal{E}_1 \frac{1}{k_m}(\alpha_m \hat{x} + ik_x \hat{z})e^{ik_x x - \alpha_m z}e^{-i\omega t}$$

$$\vec{\mathcal{E}}_2 = \mathcal{E}_1 \frac{1}{k_m}(\alpha_m \hat{x} - ik_x \hat{z})e^{-ik_x x - \alpha_m z}e^{-i\omega t} \tag{A2}$$

$$\vec{\mathcal{H}}_1 = \mathcal{E}_1 \sqrt{\epsilon_m}\, \hat{y}\, e^{ik_x x - \alpha_m z}e^{-i\omega t}$$

$$\vec{\mathcal{H}}_2 = \mathcal{E}_1 \sqrt{\epsilon_m}\, \hat{y}\, e^{-ik_x x - \alpha_m z}e^{-i\omega t} \tag{A3}$$

and

$$\vec{k}_1 = k_x\hat{x} + i\alpha_m\hat{z}$$

$$\vec{k}_2 = -k_x\hat{x} + i\alpha_m\hat{z} \tag{A4}$$

where $k_x^2 - \alpha_m^2 = k_m^2 = \epsilon_m \frac{\omega^2}{c^2}$. The nonlinear polarization associated with the counterpropagating interface surface plasmons is given by

$$\vec{P}^{(2)} = \alpha[(\vec{\nabla}\cdot\vec{\mathcal{E}}_1)\vec{\mathcal{E}}_2 + (\vec{\nabla}\cdot\vec{\mathcal{E}}_2)\vec{\mathcal{E}}_1] + \beta[(\vec{\mathcal{E}}_1\cdot\nabla)\vec{\mathcal{E}}_2 + (\vec{\mathcal{E}}_2\cdot\nabla)\vec{\mathcal{E}}_1]$$

$$+ \gamma[\vec{\mathcal{E}}_1\times\vec{\mathcal{K}}_2 + \vec{\mathcal{E}}_2\times\vec{\mathcal{K}}_1]. \tag{A5}$$

The bulk contribution to the nonlinear polarization, obtained by using Eqs. (A2) to (A4) to evaluate $\vec{P}^{(2)}$, is given by

$$\vec{P}^{(2)}_{\text{bulk}} = \hat{z}\mathcal{E}_1^2\left[\frac{2i\beta\alpha_m k_x^2}{k_m^2} + \frac{2\gamma\alpha_m\sqrt{\epsilon_m}}{k_m}\right]e^{-2\alpha_m z}e^{-2i\omega t}. \tag{A6}$$

In addition, in the presence of the interface at $z = 0$, there is also a surface contribution to the nonlinear driving force,

$$\vec{P}^{(2)}_{\text{surface}} = \lim_{\eta\to 0}\int_{-\eta}^{\eta}\vec{P}^{(2)}dz. \tag{A7}$$

Physically, the surface polarization term arising from $\vec{P}^{(2)}$ can be interpreted as a single dipole layer lacking inversion symmetry. To evaluate Eq. (A7), because both $\vec{\mathcal{E}}$ and $\vec{\mathcal{K}}$ are finite and bounded at the interface $z = 0$, in the limit $\eta \to 0$, the M2 term, as well as terms of the

form $\mathcal{E}_i \frac{\partial}{\partial x} \mathcal{E}_j$, vanish; only terms containing $\frac{\partial}{\partial z}$ give nonzero contributions. In particular,

$$\vec{P}^{(2)}_{surf} = \lim_{\eta \to 0} \int_{-\eta}^{\eta} dz \left\{ \alpha \left[\left(\frac{\partial}{\partial z} \mathcal{E}_{1z} \right) \vec{\mathcal{E}}_2 + \left(\frac{\partial}{\partial z} \mathcal{E}_{2z} \right) \vec{\mathcal{E}}_1 \right] \right.$$

$$\left. + \beta \left[\left(\mathcal{E}_{1z} \frac{\partial}{\partial z} \right) \vec{\mathcal{E}}_2 + \left(\mathcal{E}_{2z} \frac{\partial}{\partial z} \right) \vec{\mathcal{E}}_1 \right] \right\} . \tag{A8}$$

Using the component form of the fields and using the boundary condition requiring that $(\vec{D})_\perp$ be continuous to relate the fields at $\pm \eta$, one finds

$$\vec{P}^{(2)}_{surf} = \hat{z}\, \mathcal{E}^2_{1z}(0^+) \left(\varepsilon_m^2 - 1 \right) (\alpha + \beta) e^{-2i\omega t} . \tag{A9}$$

Thus, for counterpropagating surface plasmons at a metal-air interface, the nonlinear polarization, including surface and bulk contributions, has a nonzero component only along $\hat{z}$, and therefore cannot radiate a coherent second harmonic beam propagating along $\hat{z}$. This conclusion results strictly from the symmetry properties of the metal and the geometry of the input surface plasmon fields.